Assimilation of moored velocity data in a model of coastal wind-driven circulation off Oregon: Multivariate capabilities

Alexander L. Kurapov, J. S. Allen, G. D. Egbert, R. N. Miller, P. M. Kosro, M. D. Levine, T. Boyd, and J. A. Barth

College of Oceanic and Atmospheric Sciences, Oregon State University, Corvallis, Oregon, USA

Received 17 May 2004; revised 23 September 2004; accepted 25 January 2005; published 29 September 2005.

[1] Horizontal current measurements from an array of moored acoustic Doppler profilers are assimilated sequentially into a model of coastal wind-driven circulation off Oregon during the upwelling season of May–August 2001. Model results are compared against independent moored and ship survey data to document a positive effect of velocity data assimilation (DA) on other oceanic variables of interest such as the sea surface height (SSH), temperature, potential density, surface salinity, and near-bottom turbulence parameters. Significant improvement is achieved for the nearshore SSH even when data are assimilated from only two moorings at an alongshore distance of 50 km from the SSH verification site. At 45°N, in an area of simple shelf bathymetry with relatively small alongshore variations, the model (even without DA) provides a good description of the isopycnal structure on a cross-shore section. At 44.2°N, over complicated bathymetry, velocity DA may improve the slope of isopycnals but at the same time not necessarily the density values themselves. Data assimilation based on a time-invariant representation of the forecast error covariance may inhibit spatial variability on horizontal scales smaller than the assumed forecast error decorrelation scale. An experiment involving assimilation of both velocity and moored salinity measurements demonstrates that moored velocity DA improves transport of buoyant surface water. The level of improvement in the near-bottom turbulent dissipation and bottom stress found with the DA model indicates that it is suitable for future studies of spatial and temporal variability in the bottom boundary layer off Oregon.

Citation: Kurapov, A. L., J. S. Allen, G. D. Egbert, R. N. Miller, P. M. Kosro, M. D. Levine, T. Boyd, and J. A. Barth (2005), Assimilation of moored velocity data in a model of coastal wind-driven circulation off Oregon: Multivariate capabilities, *J. Geophys. Res.*, *110*, C10S08, doi:10.1029/2004JC002493.

1. Introduction

[2] The ability to predict unobserved oceanic variables is one of the powerful aspects of data assimilation (DA), a set of techniques that combine observations with a dynamical model to improve estimates of the ocean state. The study presented here continues work of *Kurapov et al.* [2005a] (hereinafter referred to as K05) that describes assimilation of horizontal velocities from moored acoustic Doppler profilers into a model of coastal wind-driven circulation off Oregon. The study period is May–August 2001 when the wind drives a predominantly southward alongshore current and upwelling near the coast, a typical summer regime off Oregon [*Oke et al.*, 2002a, 2002b]. K05 studied the effect of DA on the velocity field at alongshore distances up to 90 km from sites where data were assimilated. The focus of the present paper is on multivariate capabilities of this DA system, i.e., on how assimilation of velocity data affects other oceanic variables of interest, e.g., sea surface height (SSH), temperature, salinity, and turbulent dissipation. Data used here were collected through efforts of the Coastal Ocean Advances in Shelf Transport (COAST) program (moorings, hydrographic ship surveys, and land-based high-frequency radars), the Global Ocean Ecosystem Dynamics (GLOBEC) program (an acoustic Doppler profiler mooring), and the National Oceanic and Atmospheric Administration (NOAA) service (tide gauge data).

[3] Data assimilation (DA) has been under development in meteorology for several decades [*Daley*, 1993]. For global ocean applications, sustained DA efforts have been undertaken with the goal of understanding the general circulation and its transport variability [*Stammer et al.*, 2003]. However, for coastal applications, DA has not yet become a widespread tool for research and operations in part because data suitable for assimilation have been scarce. It is also true that coastal ocean circulation models have only recently reached a sufficient level of realism in describing flow variability at temporal scales of several

0148-0227/05/2004JC002493$09.00

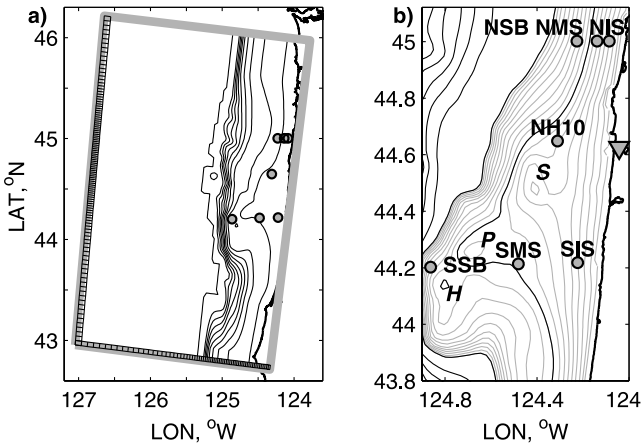

Figure 1. Maps of the Oregon shelf with circles showing mooring locations in May–August 2001. (a) Computational domain with grid cells along the western and southern boundaries showing the rectangular grid resolution; the bathymetric contour interval is 100 m. (b) A close-up view of the mid-Oregon shelf; the bathymetric contour interval is 100 m for the black lines and 10 m for the half-tone lines (from 10 to 200 m). *S*, *P*, and *H* denote banks: Stonewall, Perpetua, and Heceta; an upside-down triangle shows location of the NOAA tide gauge (South Beach, Oregon).

days and spatial scales on the order of 10 km or less [e.g., *Oke et al.*, 2002b; *Gan and Allen*, 2002]. Presently, an initiative to establish a network of ocean observatories along the U.S. coasts motivates advancement of coastal circulation models with DA capability and verification of their capabilities using data sets available today. In the context of coastal DA, a number of studies have been undertaken assimilating high-frequency (HF) radar surface currents [*Lewis et al.*, 1998; *Breivik and Sætra*, 2001; *Oke et al.*, 2002a; *Kurapov et al.*, 2003], moored temperature profiles [*Chen and Wang*, 1999], and physical and biological fields from hydrographic surveys [*Beşiktepe et al.*, 2003]. Focusing on multivariate aspects, *Chen and Wang* [1999] demonstrated the value of temperature assimilation in the upper 100 m for prediction of the seasonal circulation in the Santa Barbara channel.

[4] The best estimate of the ocean state for the period of the COAST summer field program should in principle be obtained by assimilation of all available data. In practice, there are many issues that would need to be addressed to optimally use the full data set, e.g., the relative weighting of different data types, model-data compatibility, etc. Rather than focusing on these issues, here we use the extensive and unique COAST data sets to evaluate the performance of a prediction system assimilating only velocity data from moored sensors. While not all the data types available from the COAST program will become routine as part of emerging coastal ocean observatories, moored acoustic velocity profilers will certainly be one of their backbone components. Findings from this study can demonstrate the net effect of assimilation of moored velocity data and provide guidance for building an optimal DA system in support of coastal ocean observatories. Results of model evaluation against data that are not assimilated should improve our confidence in solutions for the periods when validation data are not available.

[5] In this manuscript, the data assimilative model is described in section 2 and the basic model-produced circulation patterns on the Oregon shelf in section 3. Then, in section 4, DA results are compared against nearshore sea surface height time series data from a tide gauge. In section 5, the effect of velocity DA on temperature variability is studied using measurements from moored sensors. In section 6, the effect of DA on the isopycnal structure, both in horizontal and vertical transects, is assessed using ship survey hydrographic data. In section 7, experiments involving salinity measurements from moored sensors, in addition to velocity measurements, are described to show how velocity DA helps to control alongshore advection of the surface buoyant water. In section 8, modeled near-bottom turbulence parameters are compared against those derived from microstructure measurements in the bottom boundary layer (BBL). Section 9 provides a summary. Where possible, we not only document statistical improvements, but also assess the dynamical significance of the changes caused by DA.

2. Data Assimilative Model

[6] The model configuration is similar to that used by *Oke et al.* [2002a, 2002b; see also K05] where implementation details, omitted here, can be found. The dynamics are based on the Princeton Ocean Model (POM) [*Blumberg and Mellor*, 1987], a fully nonlinear, free-surface, hydrostatic model with a subgrid turbulence parameterization scheme [*Mellor and Yamada*, 1982]. The model domain extends 220 km offshore and 350 km alongshore (Figure 1a). The grid is rectangular with the horizontal (x, y) axes rotated 7° clockwise from north. The x axis is then directed across-shore, toward the coast, and the y axis is directed alongshore, positive to the north. Velocity components in these directions are u and v, respectively. The maximum grid resolution is 2 km in the vicinity of Newport (44.6°N), with decreased resolution toward the western, northern and southern boundaries. The model uses terrain-following coordinates in the vertical, with 31 σ layers, including 8 concentrated near the surface and 4 near the bottom in order to resolve boundary layers. The alongshore boundary conditions are periodic, with the bathymetry and coastline smoothed and matched near the south and north ends of the domain. Although solutions obtained with this periodic channel geometry have limitations, extensive model-data comparisons documented by *Oke et al.* [2002b] have shown that many important aspects of the shelf flow are successfully represented in this domain. The reason for this success is that off Oregon the coastal currents are strongly wind driven, with much of the mesoscale behavior on the shelf dominated by local flow-topography interaction. The evaluation of model-only solutions of *Oke et al.* [2002b] included favorable comparisons with measurements of depth-dependent currents and temperatures from moorings, of surface currents from shore-based HF radars, and of hydrographic measurements from repeated Minibat conductivity-temperature-depth (CTD) sections as well as from horizontally extensive SeaSoar CTD surveys. The encouragingly good agreement between the model and

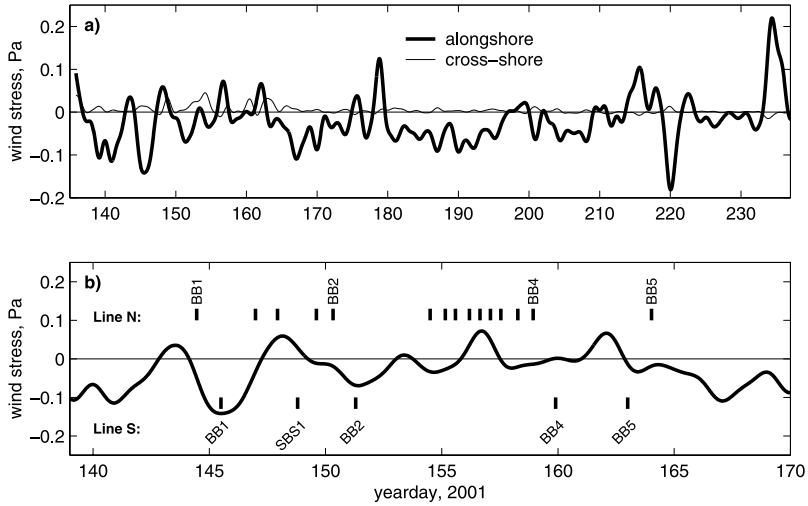

Figure 2. Wind stress (a) for the period of COAST 2001 upwelling experiment and (b) for the beginning of the field program with marks showing times of SeaSoar hydrographic transects near lines N and S [*Barth et al.*, 2003].

observations found in that study motivates the use of a similar model setup for the DA experiments reported here.

[7] The model is forced with alongshore wind stress and surface heat flux. Wind speed, short wave insolation, air temperature, and relative humidity necessary for the calculation of wind stress and heat flux were measured at a meteorological buoy located midshelf at latitude 45°N. In the model, these inputs are assumed to be spatially uniform. Since our focus is on subinertial wind-forced ocean variability, the wind stress (Figure 2) and the measured variables used for heat flux computation are low-pass filtered with half amplitude cutoff of 40 hours. The mooring data used for assimilation, and the observed and model time series used for statistical analysis, are also low-pass filtered.

[8] Implementation of more realistic, spatially varying atmospheric forcing, for instance, obtained from a regional atmospheric model, could potentially reduce the model error, but would require an open boundary formulation in place of the periodic channel setup. One of the major problems with the open boundaries in our case stems from the fact that the dominant direction of the energetic alongshore current in summer is southward, opposite to the northward direction of propagation of coastally trapped waves. That situation has been studied by *Gan and Allen* [2005] and *Gan et al.* [2005] who have formulated and tested suitable open boundary conditions and who have applied them in the model forced with spatially varying winds from a regional atmospheric model. Our experience has suggested that data assimilation may bring additional complications with open boundary conditions, for example, affect radiation properties of the open boundary [*Kurapov et al.*, 2003]. The use of data assimilation methodology to help provide useful open boundary conditions for coastal applications is a difficult research problem that is currently under investigation. So, for our present study, we retain the more robust, periodic channel model and use velocity data assimilation to filter the error associated with different model error sources in the area of our mooring array.

[9] Data are assimilated using an optimal interpolation (OI) method, as described by K05. By means of OI, horizontal velocities in the computational domain are corrected sequentially every quarter of an inertial period (approximately 4 hours) based on model-data differences. Note that correction is applied only to horizontal velocities while other model variables (sea surface height, T, S, etc.) are allowed to adjust dynamically. The tradeoff between the modeled and observed velocities is controlled by forecast and data error covariances, which are time invariant in OI. The choice of the forecast error covariance is estimated based on the methodology described by *Kurapov et al.* [2002] and K05. To inhibit spurious high-frequency oscillations caused by imposed instantaneous changes in the velocity fields, an incremental approach is taken, such that the correction is applied gradually, in small increments over the analysis window of a quarter of the inertial period.

[10] Locations of moorings used in this study are shown in the map of the central part of the domain (Figure 1b). The northern line of moorings, referred to as line N, is at 45°N, and includes moorings NSB (North Shelf Break), NMS (North Mid-Shelf), and NIS (North Inner Shelf). Correspondingly named moorings SSB, SMS, and SIS form line S at 44.2°N. These six moorings are a part of the COAST experiment. The seventh, GLOBEC mooring (NH10) is installed midshelf off Newport (44.65°N). The acoustic Doppler profilers measured horizontal velocity in 2 or 4 m vertical bins at a sampling interval of 120 s [*Boyd et al.*, 2002] (available at http://damp.coas.oregonstate.edu/coast/moorings.shtml). Velocity observations are obtained as close as approximately 15 m to the sea surface and bottom at NSB and SSB, and 10 m at all the other sites.

[11] Before the start of DA, the model is spun-up from a state of rest (zero velocities and horizontally uniform stratification). Initial profiles of potential temperature T and salinity S are shown in Figure 3. In the upper 100 m, they are obtained by averaging T and S from a number of R/V *Wecoma* Big Box (BB) hydrographic transects, year days 144–154, 2001. BB cruise tracks are shown in

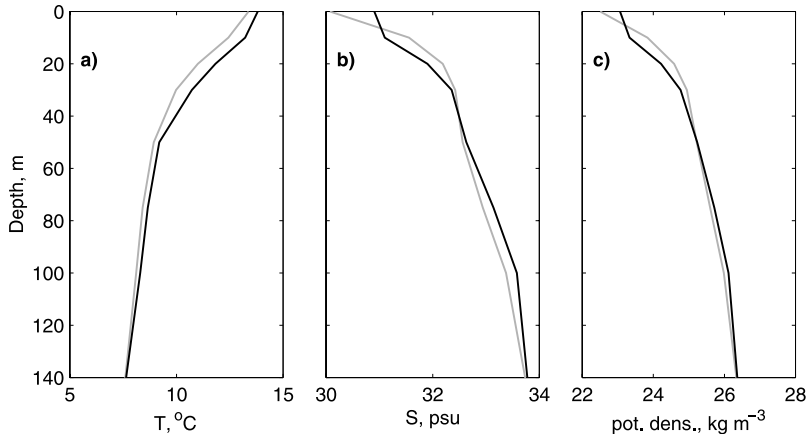

Figure 3. Initial profiles of (a) potential temperature, (b) salinity, and (c) potential density. Black lines are average profiles from SeaSoar conductivity-temperature-depth (CTD) measurements at offshore locations from the Big Box surveys (Figure 11). Half-tone lines are averages of hydrographic measurements at a station 45 nautical miles offshore off Newport in June (1961–1971).

Figure 11. To obtain the initial profiles, only data at the offshore track segments of the BB surveys were used. At depths below 100 m the profiles are matched to the mean observed profiles from June 1961–1971, at a station 45 nautical miles offshore of Newport. The model is initially forced with a constant time-invariant alongshore southward wind stress of 0.05 Pa for 10 days, followed by 5 days with no wind. As a result of this 15 day initialization, the velocity and density fields are balanced and are qualitatively close to average summer upwelling conditions on the Oregon shelf. Next, the model is continued to be spun-up with observed winds and heat flux for 3 days, to bring the model into a more realistic state before the beginning of DA. After that, before the analysis of the solution begins, the model is run with observed forcing and DA for 5 more days to filter the model error that may be associated with initial conditions. Unless otherwise specified, imposition of the observed forcing starts on day 138 (18 May). Data assimilation starts on day 141 (21 May), when data from all the COAST moorings are available. The model output is analyzed starting on day 146 (26 May). The computations last until day 237 (25 August), after which

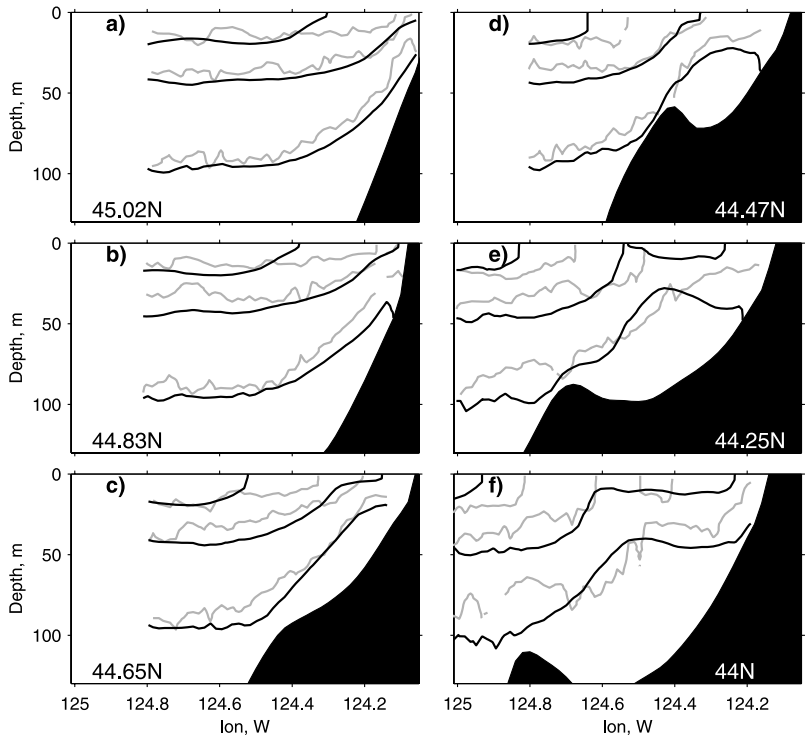

Figure 4. Contours of potential density σ_θ = 24, 25, and 26 kg m^{-3} in vertical sections of the SeaSoar survey Big Box 1 (BB1) (days 144.4–145.8). SeaSoar data are half-toned, and modeled contours (no DA) are black.

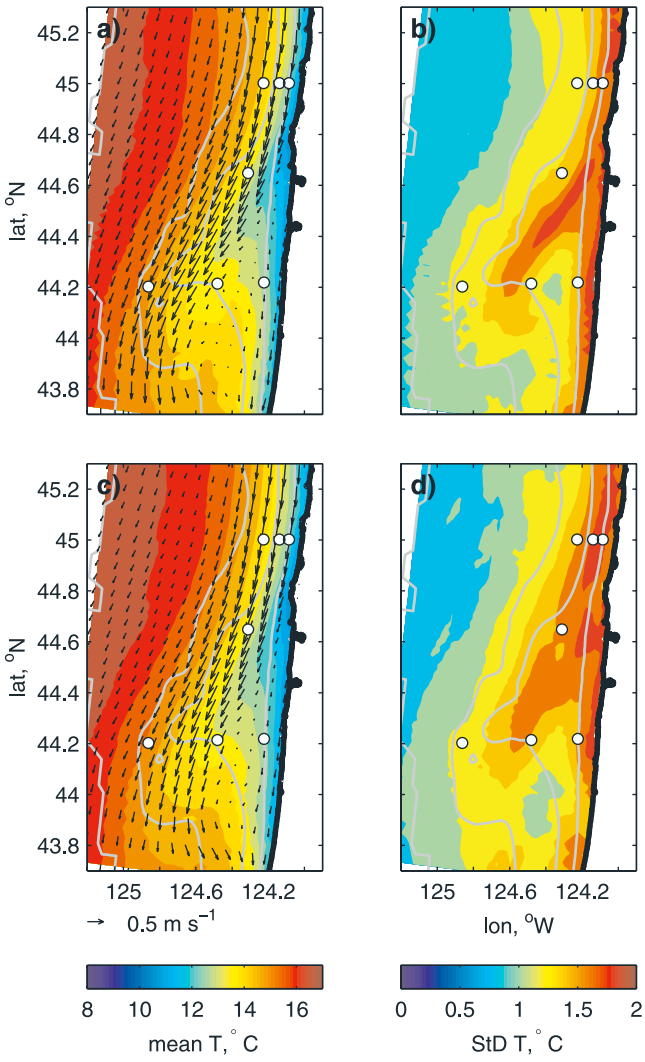

Figure 5. (left) Time-averaged surface velocity (vectors) and temperature (color) fields, days 146–191, and (right) corresponding temperature standard deviation. Upper plots correspond to the model without DA and lower plots to case DA (N+S). Circles are the mooring locations. Bathymetric contours are at 50, 100, 200, and 1000 m. Velocity vectors are shown at each 3rd grid cell.

the COAST moorings were recovered. The model solution without DA, used as a benchmark in this study, was initialized similarly.

[12] Since the model solution may be sensitive to the initial conditions and details of the spin-up [*Oke et al.*, 2002b], we performed a series of sensitivity studies and verified that the initialization procedure described above yields a good agreement between the model (without DA) and measurements of potential density σ_θ from the SeaSoar towed undulating platform made in a number of cross-shore sections on days 144–146, close to the beginning of the analysis period [*Barth et al.*, 2003; *Castelao and Barth*, 2005] (Figure 4). Note that small-scale spatial variability in the SeaSoar data may be associated with high-frequency internal wave motions not represented in our model.

[13] Fresh water input from the Columbia River, at 46.2°N, is not included in our model. Lighter water associated with Columbia River intrusion, found in the measurements (section 7), is confined to the upper 10–15 m. Although the error in the velocity field certainly affects the transport of surface buoyant water from the Columbia River (see section 7), we presume that in the area of the mooring array, 140 km south of the river mouth, the dynamical effect of these intrusions, e.g., on the velocities, is not substantial at the spatial and temporal scales under consideration.

3. Summer Circulation Regime off Oregon

[14] Forced by typically southward alongshore wind stress (see Figure 2a), a southward jet develops over the continental shelf. The time-averaged surface current is shown in Figure 5a. The jet is generally deflected offshore from the coast at 44.8°N, following bathymetric contours where the shelf widens. At the south edge of Heceta Bank (43.9°N), where the shelf narrows again, the flow crosses bathymetric contours and separates from the shelf. Cold water is upwelled near the coast, as can be seen in the time-averaged SST (near 11°C) shown in Figure 5a. Maximum variability in the model SST is evident near the coast and along the path of the upwelling jet, with standard deviation near 2°C (Figure 5b). Note that the 11°C and 9°C water is initially at 30 m and 50 m depths, respectively (see Figure 3a). Hydrographic and biochemical samplings on the Oregon shelf show that conditions of the summer 2001 season were close to climatology [*Freeland et al.*, 2003; *Wheeler et al.*, 2003; *Castelao and Barth*, 2005].

[15] The time series of depth-averaged alongshore velocity at mooring locations are shown in Figure 6, with observations as a shaded line and the model without DA as a thin black line. Model-data statistics comparing velocities at the mooring sites are given in Table 1. The amplitude of the complex correlation (defined as by *Kundu* [1976]) between modeled and observed depth-averaged currents for days 146–237 is reasonably high at the moorings of line N (0.64–0.69), but is lower at NH10 (0.48), SSB (0.24), SMS (0.07), and SIS (0.52). K05 showed that assimilation of velocities from either line N or S improves model-data velocity correlation and RMS error at the other line. However, when data are assimilated only on line N, the mean depth-averaged current at SSB remains larger than observed. When data are assimilated only on line S, mean currents on line N are weaker than observed. For this study, to constrain the current intensity and improve velocity statistics in the area between lines N and S, currents from all 6 moorings on both lines are assimilated in the model. This is chosen as the standard DA case, referred to as Case DA (N+S).

[16] The velocity data from mooring NH10, in the middle of the area, are not assimilated in the standard case. These measurements are used to verify that the solution, fit closely to data to the north and south, remains reliable between the two mooring lines. Fitting the data too tightly at the two cross-shore lines may result in discontinuities and spurious eddies in the vicinity of the data sites. That could possibly happen if features resulting from overfitting data on one line are advected (preferentially to the south) or propagated with

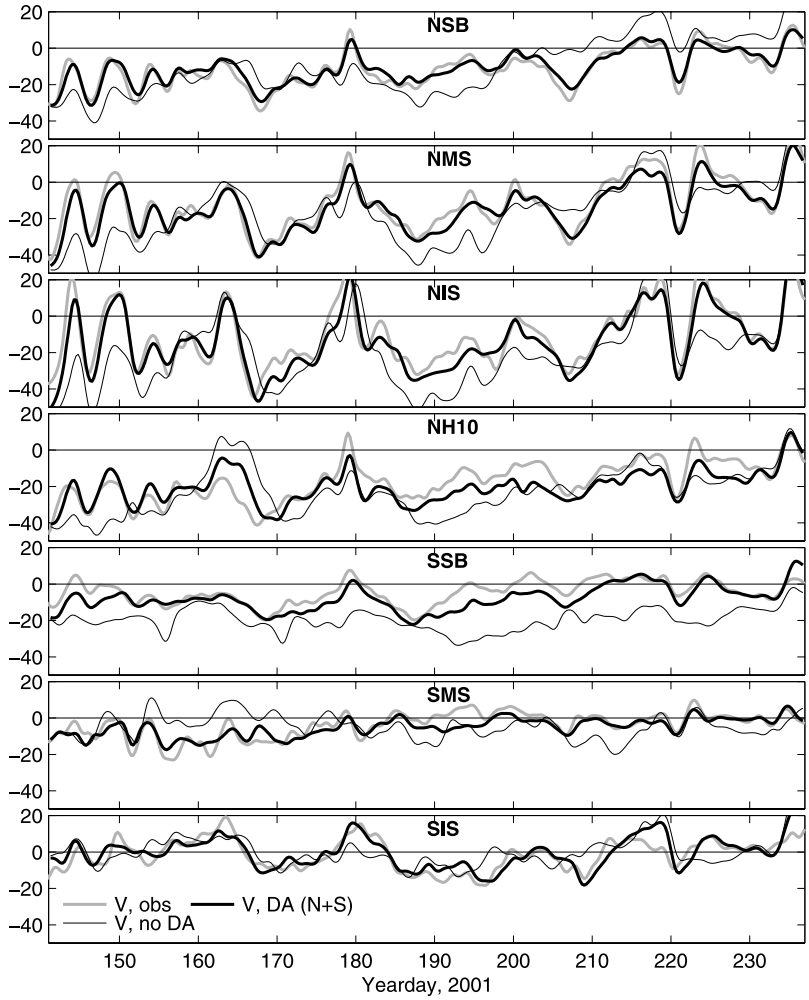

Figure 6. Time series of the depth-averaged alongshore currents at mooring locations: observations (shaded lines), no DA (thin lines), and DA (N+S) (bold lines). For model-data statistics, see Table 1.

coastally trapped waves (to the north) to deliver erroneous information to the other line, inconsistent with local data. Allowing for the errors at the level of 3–5 cm s^{-1} in the forecast and 10 cm s^{-1} in the data (K05) avoids these problems. As evidence of the beneficial effect of DA, the modeled velocity at NH10 is closer to the observed velocity (see Figure 6 and Table 1), with the amplitude of the model-data complex correlation for the depth-averaged current increased from 0.48 to 0.74. At the sites where data are assimilated, model-data velocity correlation amplitude for the DA solution is near 0.95 (line N) and 0.8 (line S). The solution-data RMS differences range from 3.4 to 5.6 cm s^{-1} at the assimilated sites and is 6.6 cm s^{-1} at NH10 (Table 1). As a result of DA, model velocity has been improved throughout the water column at the assimilated sites and NH10. Velocity variability in the vertical is discussed in more detail by K05.

[17] As reported by K05, the model does not reproduce fluctuations of the jet evident in satellite SST images in the second half of the study period (although data assimilation provides improvement to velocities at NH10 during that period). For this reason, model-data comparisons using moored, ship survey, and HF radar observations are performed here also only for the first half of the study period.

[18] Model surface currents can be compared against observations of surface velocities from coastally based HF radars. Five HF radars were in operation off Oregon during spring–summer 2001 measuring radial components of surface velocities at a distance of <50 km from the instruments. These data were processed into eastward and northward velocities on a 2 × 2 km regular grid and low-pass filtered. In the alongshore direction, these observations cover the

Table 1. RMS Error and the Amplitude of the Complex Correlation Between Modeled and Observed Velocity Time Series at Mooring Locations, Days 146–237, Model Without Data Assimilation (No DA) and Case DA (N+S)[a]

Case	NSB	NMS	NIS	NH10	SSB	SMS	SIS
			RMS Error				
No DA	9.0	9.9	12.6	10.3	13.8	9.7	6.8
DA (N+S)	3.4	4.4	5.6	6.6	5.1	4.9	4.8
			Correlation Amplitude				
No DA	0.64	0.69	0.69	0.48	0.24	0.07	0.52
DA (N+S)	0.94	0.96	0.94	0.74	0.80	0.81	0.80

[a]The RMS error is found by time averaging squared model-observation velocity differences at each profiler bin and then by vertically averaging. The correlation is for the depth-averaged currents.

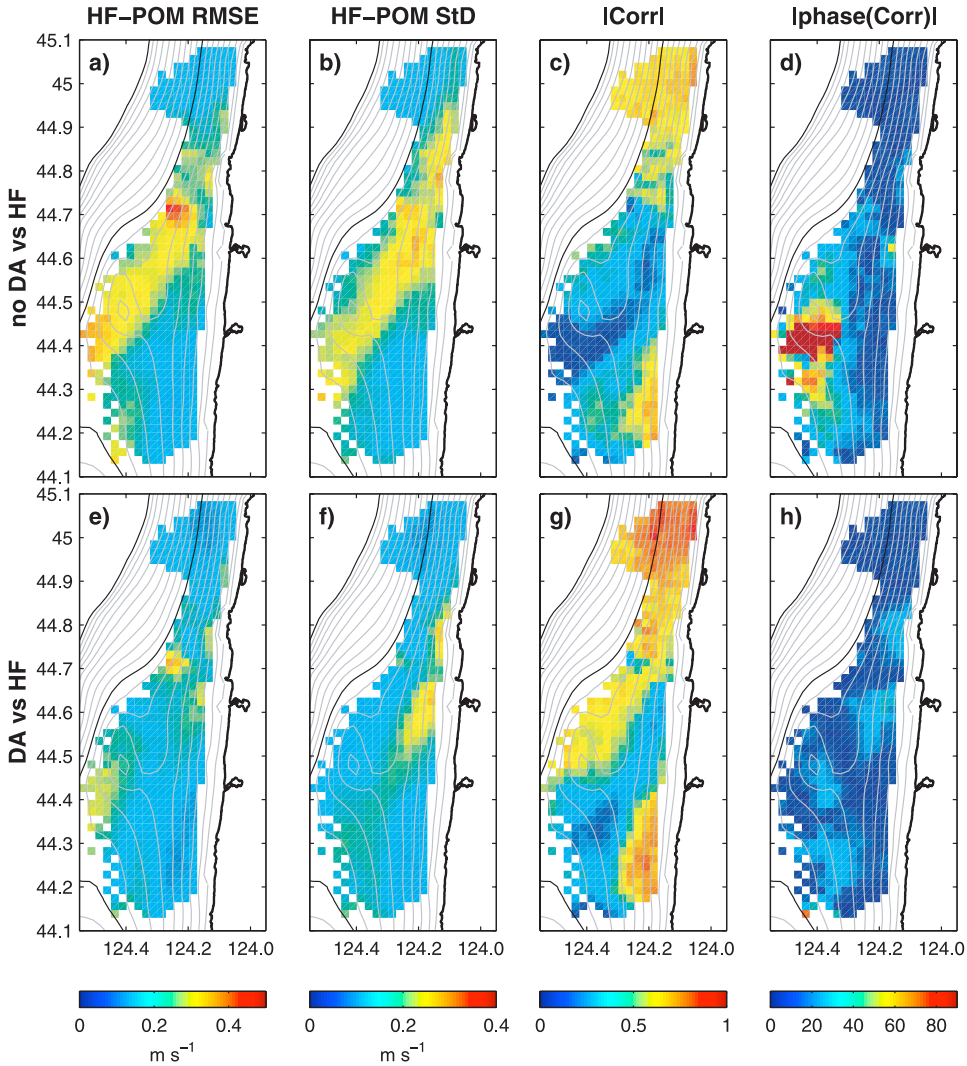

Figure 7. HF radar versus model near-surface current statistics, days 146–191, (top) no DA and (bottom) DA. (a, e) RMS error. (b, f) Standard deviation of model-data differences (equivalent to RMS error with means taken out). (c, g) Amplitude and (d, h) phase of complex correlation. Bathymetric contour intervals are 10 m, from 10 to 200 m, with the 100 and 200 m contours in black.

area between the two mooring lines, although HF radar coverage does not extend offshore as far as mooring SSB. In Figure 7, the model velocities vertically averaged in the top 1 m below the sea surface are compared with the HF radar data in terms of model-data RMS error, standard deviation of model-data differences (equivalent to the RMS error of demeaned time series), and amplitude and phase of the complex correlation coefficient (Figure 7). Assimilation of mooring velocities provides a noticeable improvement to the solution in terms of all these criteria.

4. Effect of Moored Velocity Assimilation on Sea Surface Height (SSH)

[19] Since wind-induced, subinertial variability in SSH on the inner shelf may affect estuarine circulation and ultimately estuarine-ocean water mass exchange [*Wong and Valle-Levinson*, 2002], it is important to assess the ability of a DA model to improve SSH near the coast. Here, modeled SSH is compared against NOAA tide gauge data at South Beach, Newport, marked as a triangle in Figure 1b. To compare the modeled and observed SSH, the tide gauge data are corrected for barometric pressure, and both observed and modeled time series are low-pass filtered and demeaned (Figure 8). SSH model-data statistics for a number of different computational cases are given in Table 2. In case DA (N+S), assimilation of velocities significantly improves the SSH model-data correlation and decreases the RMS error. This should be expected since DA provides a constraint on the alongshore surface current that is in approximate geostrophic balance with the cross-shore SSH gradient [see *Oke et al.*, 2002c]. The SSH improvement in case DA (N+S) is comparable to that in case DA (NH10), when velocity measurements are assimilated only from NH10, the site closest to the SSH measurement location (the SSH time series for this case is shown as a dotted line in Figure 8). The improvements found for DA cases (NSB+NMS) and (SSB+SMS), where data are assimilated from just two moorings on a single cross-shore line, suggest that SSH can also be better

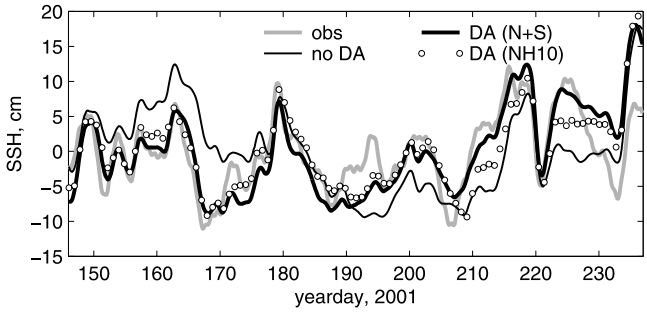

Figure 8. Time series of sea surface height near the coast at 44.62°N (at the location marked with a triangle in Figure 1b): observations at the NOAA tide gauge station 9435380 (shaded line), no DA (thin line), DA (N+S) (bold line), and DA (NH10) (circles). The data-model statistics for these and some other DA cases are given in Table 2.

represented by assimilation of currents from a small number of moorings at remote sites (see Table 2).

[20] Improvement in the nearshore SSH during days 156–178 (see Figure 8) is associated with DA control of the location of the SSH depression in the coastal jet separation zone south of 44.8°N. This is illustrated with maps of SSH and surface velocities averaged over day 166 (Figures 9a and 9b), during a strong upwelling event. On this day, in the model without DA, the local minimum of SSH is obtained over Stonewall Bank (124.4°W, 44.5°N) (Figure 9a). This local feature is in approximate geostrophic balance with the surface current that tends to flow around the bank. Data assimilation yields a more uniform surface velocity field crossing isobaths and flowing over the bank (Figure 9b), which is, e.g., in closer agreement with the observed HF radar surface currents (Figure 9c). The SSH is dynamically adjusted to the velocity correction such that the depression zone is moved farther to the south (Figure 9b). At the same time, DA reduces the SSH nearshore, where the measurements were taken.

[21] Pressure gradients associated with spatial variations in the SSH over Stonewall Bank are consistent with flow variability throughout the water column, and with the flow regime over the bank. For instance, in the solution without DA, on day 166, near-bottom horizontal currents tend to go around the bank (Figure 9d), with the weak northward flow on its eastern flank and low currents over its top. In the DA solution, the near-bottom current of 7 cm s^{-1} flows over the bank in the southwest direction. Thus assimilation of moored velocities has changed the flow regime over the bank, possibly providing conditions for small-scale hydraulic flows over the fine bathymetry, which are not resolved in our model, but which have been observed over Stonewall Bank by *Nash and Moum* [2001].

5. Effect of Moored Velocity Assimilation on Temperature

[22] Temperature time series measurements are available throughout the water column at all six COAST moorings of lines N and S. Statistics comparing these data to model solutions without DA and with DA (N+S) for days 146–191 are shown versus depth in Figure 10. Data assimilation does not significantly change modeled time-averaged potential temperature or standard deviations, which are already close to observed profiles. At the surface, maps of the time-averaged temperature and its standard deviation from the DA solution are also qualitatively similar to those from the model without DA (see Figure 5). However, throughout the water column at most mooring sites, DA improves the agreement of model and observed temperature fluctuations, as estimated by the improvements in the standard deviation of model-data temperature differences (equivalent to the RMS error of model and observed time series with means taken out) and model-data correlations.

[23] Although statistical improvements in the temperature are moderate on average over the study period, velocity DA may yield dynamically significant adjustments in the temperature field (and hence the potential density σ_θ) on the event scale. One example is given in Figures 9d and 9e, where the near-bottom σ_θ average for day 166 is shown in color. In the DA case (Figure 9e), in contrast to the case without DA (Figure 9d), near-bottom currents apparently advect water of $26 < \sigma_\theta < 26.4$ kg m^{-3} over the bank. A more detailed analysis of the flow variability near the bottom, including a discussion of the dynamical effects of DA, is presented by *Kurapov et al.* [2005b], where velocity DA is shown to control the intensity and timing of events of local upwelling and mixing on the midshelf east of Stonewall Bank.

6. Effect of Moored Velocity Assimilation on Isopycnal Structure

[24] A series of high-resolution hydrographic surveys were performed in May–June 2001 using a SeaSoar towed undulating platform equipped with a CTD instrument [*Barth et al.*, 2003; *Castelao and Barth*, 2005]. Processed T and S data are mapped in vertical sections along ship tracks for depths ranging from 1 to 121 m below the surface, with a grid resolution 1.25 km in the horizontal and 2 m in the vertical. The observational program included four Big Box (BB) surveys between 43.75°N and 45.25°N (see survey tracks in Figure 11) and a number of surveys focused on smaller shelf areas. Times of SeaSoar transects made next to mooring lines N and S are shown in Figure 2b.

[25] Figure 11 shows horizontal maps of σ_θ at 35 m below the surface from four SeaSoar BB surveys (upper plots), the model without DA (plots in the middle row) and case DA (N+S) (lower plots). Note that small-scale variability in the observed maps may in part result from plotting, since data are noisy and available only along the ship tracks. To compare model and data maps, the model fields are sampled in space and time the same as the SeaSoar

Table 2. RMS Error and Correlation of Modeled and Observed SSH Time Series at the Coastal Tide Gauge Station at 44.62°N, Days 146–237

Case	RMS Error, cm	Correlation
No DA	5.4	0.51
N+S	3.8	0.78
NH10	3.9	0.73
NSB+NMS	4.0	0.68
SSB+SMS	3.4	0.77

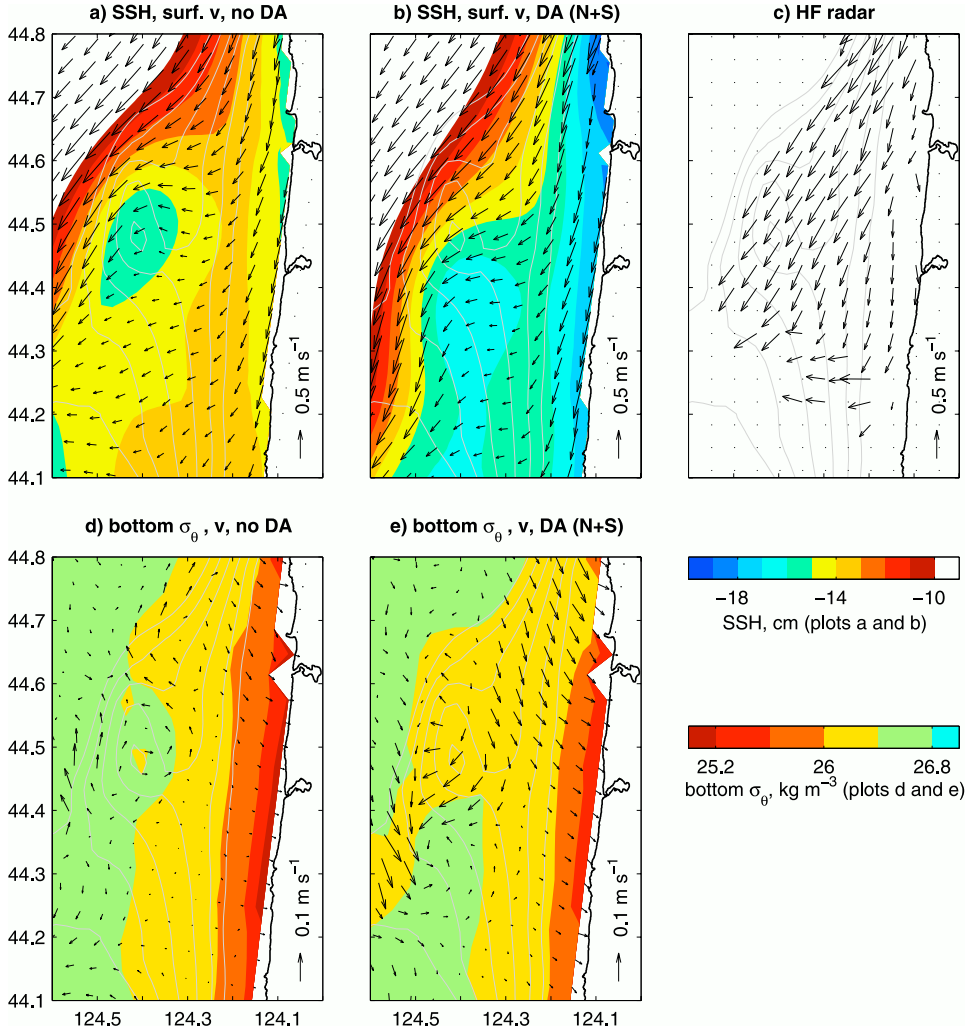

Figure 9. Dynamical effect of DA onto SSH, surface, and bottom horizontal currents and bottom σ_θ in the area near Stonewall Bank (124.4°W, 44.5°N), shown in daily averaged fields (day 166): (a) SSH and surface (u, v), no DA; (b) SSH and surface (u, v), DA (N+S); (c) HF radar observed surface velocities; (d) bottom σ_θ and (u, v), no DA; (e) bottom σ_θ and (u, v), DA (N+S). Bathymetric contours are from 50 to 100 m with contour interval of 10 m.

survey measurements are. In qualitative terms, the model reproduces the SeaSoar images, with a wider region of denser, upwelled water near Heceta Bank (44°N). The largest effect of velocity DA on σ_θ at this horizontal level is evident south of line S. Here DA reduces the offshore extent of upwelled water. For surveys BB2, BB4, and BB5, the model solution without DA predicts a pool of upwelled water extending offshore to shelf depths of 200 m near latitude 44°N. A cyclonic eddy near the southern flank of Heceta Bank is associated with this feature. For instance, such an eddy is evident in the snapshot of surface currents from the model (no DA) on day 152.0 (Figure 12a), the time when the ship was finishing survey BB2, cruising along the southern survey line. As shown in this surface plot, the isopycnals tend to be oriented along the jet path. The velocity DA inhibits this eddy flow (Figure 12b), and reduces the pool of upwelled water both near the surface and at 35 m depth (see Figure 11). This DA effect appears to be reasonable during BB4 and BB5, although during BB2, when a pool of dense water near Heceta Bank is seen in the SeaSoar data, the no DA σ_θ solution may be closer to the observations.

[26] Quantification of model-data differences using SeaSoar data is generally not straightforward since SeaSoar maps include additional variability that is not easy to filter from the data and that is not represented in the model (e.g., tides, solitary internal waves, Columbia River outflow). To provide quantitative model-data comparison for the horizontal density maps, we compute standard deviations of model-data differences $\mathrm{StD}(\sigma_\theta^m - \sigma_\theta^o)$ and model-data correlations $\mathrm{Corr}(\sigma_\theta^m, \sigma_\theta^o)$ using modeled and observed densities along the SeaSoar tracks at 35 m depth (Figure 13). To focus on the effects in the shelf area, only locations with depths of 50–200 m are used in this analysis. The statistics are computed separately for two areas: between mooring lines N and S (using SeaSoar BB cross-shore lines 2–6 counted from the north; see plots on the left in Figure 13), and south of mooring line S (using SeaSoar lines 6–8; see plots on the right in Figure 13). For surveys BB1, BB4, and BB5,

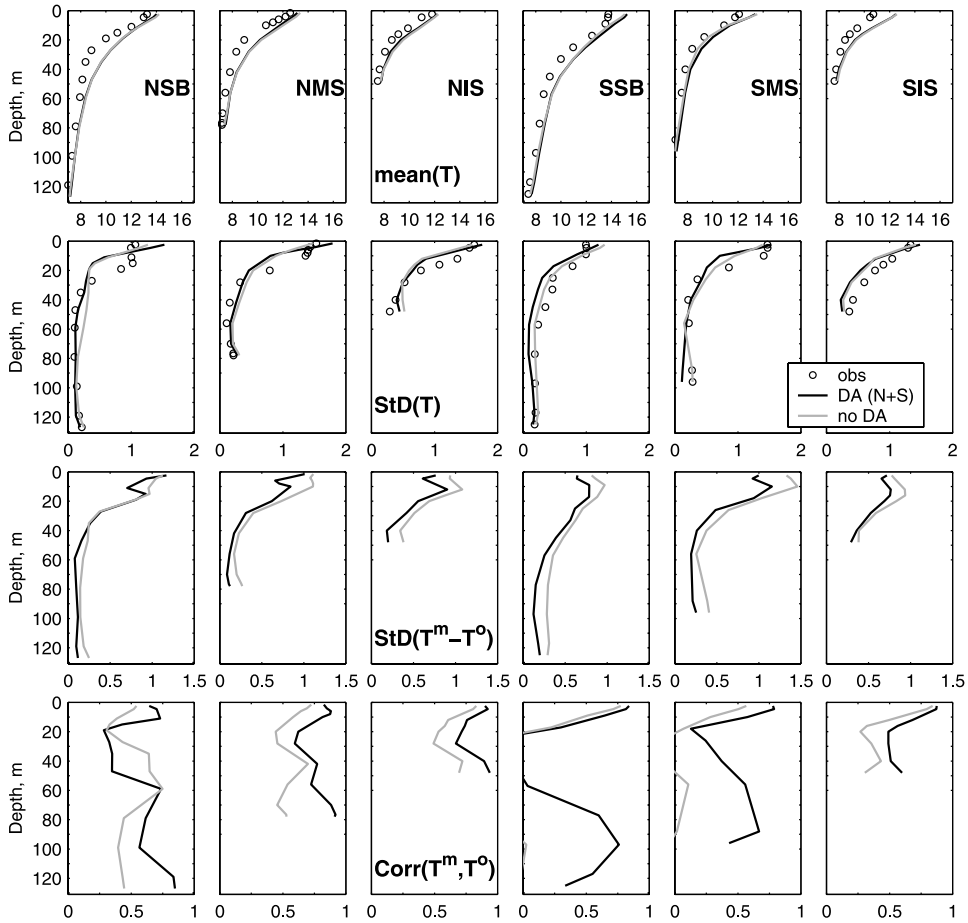

Figure 10. Statistics comparing modeled and observed potential temperature at six mooring locations for days 146–191, shown as a function of depth: observations (circles), model without DA (shaded lines), and DA (N+S) (thin lines). (top) Time-averaged *T*. (middle top) Standard deviation of *T*. (middle bottom) Standard deviation of model-data differences. (bottom) Model-data correlation.

both $\mathrm{StD}(\sigma_\theta^m - \sigma_\theta^o)$ and $\mathrm{Corr}(\sigma_\theta^m, \sigma_\theta^o)$ are improved as a result of DA in both areas. During survey BB2, model-data statistics are close for the no DA and DA solutions in an area of SeaSoar lines 2–6, although the DA model is worse than the model without DA for lines 6–8, south of line S. However, this negative effect of DA during BB2 is not as large in magnitude as the positive effect of DA south of mooring line S during surveys BB4 and BB5.

[27] The OI algorithm implemented here uses a stationary forecast error covariance $\mathbf{P}^f$ with alongshore spatial scales appropriate to "average" conditions over the study period. It is likely that during periods of jet meandering and eddy formation near Heceta Bank (see Figure 12a), the spatial decorrelation scale of the forecast error covariance in the along-jet direction is smaller than this average. Data assimilation reduces the magnitude of flow fluctuations with horizontal scales smaller than the scale implied by $\mathbf{P}^f$, as likely happened during the time of survey BB2. To better constrain the circulation in the south of our study area using the present DA algorithm, collection and assimilation of data from an additional line of moorings south of 44°N would be desirable. Possibly, a more rigorous data assimilation approach that allows for a state-dependent model solution error covariance [e.g., *Chua and Bennett*, 2001] would reduce the need for these additional moorings.

[28] We also compared modeled and observed density fields in vertical cross sections near lines N and S. Fifteen SeaSoar sections are available along line N during days 144–164. The model without DA predicts the density structure in the line N section in close correspondence with the data (see, e.g., Figure 4a). In qualitative terms, velocity DA does not modify the isopycnal structure in this section. On line S, DA has a relatively larger effect. Five SeaSoar sections, shown in Figure 14, are available there. In these sections, isopycnal contours from the model without DA (left plots) show a dome-shaped pool of denser water midshelf, east of Heceta Bank (model contours are shown in black, each 0.5 kg m^{-3}). However, such a feature is not as pronounced in the observed density contours (shaded contours, shown each 1 kg m^{-3}). Assimilation of velocity data (plots on the right side of the figure) reduces significantly the strength of this local density maximum. On Day 163 (survey BB5, bottom plots), data assimilation shifts the local maximum of potential density toward the coast, in better agreement with the SeaSoar data. At the same time, DA deepens the 26 kg m^{-3} model isopycnal, compared to the observed one. Alongshore velocity is coupled dynamically to the cross-shore density gradient, but not the density itself, so it is natural to expect that velocity DA would improve the slope of σ_θ contours, but not necessarily the

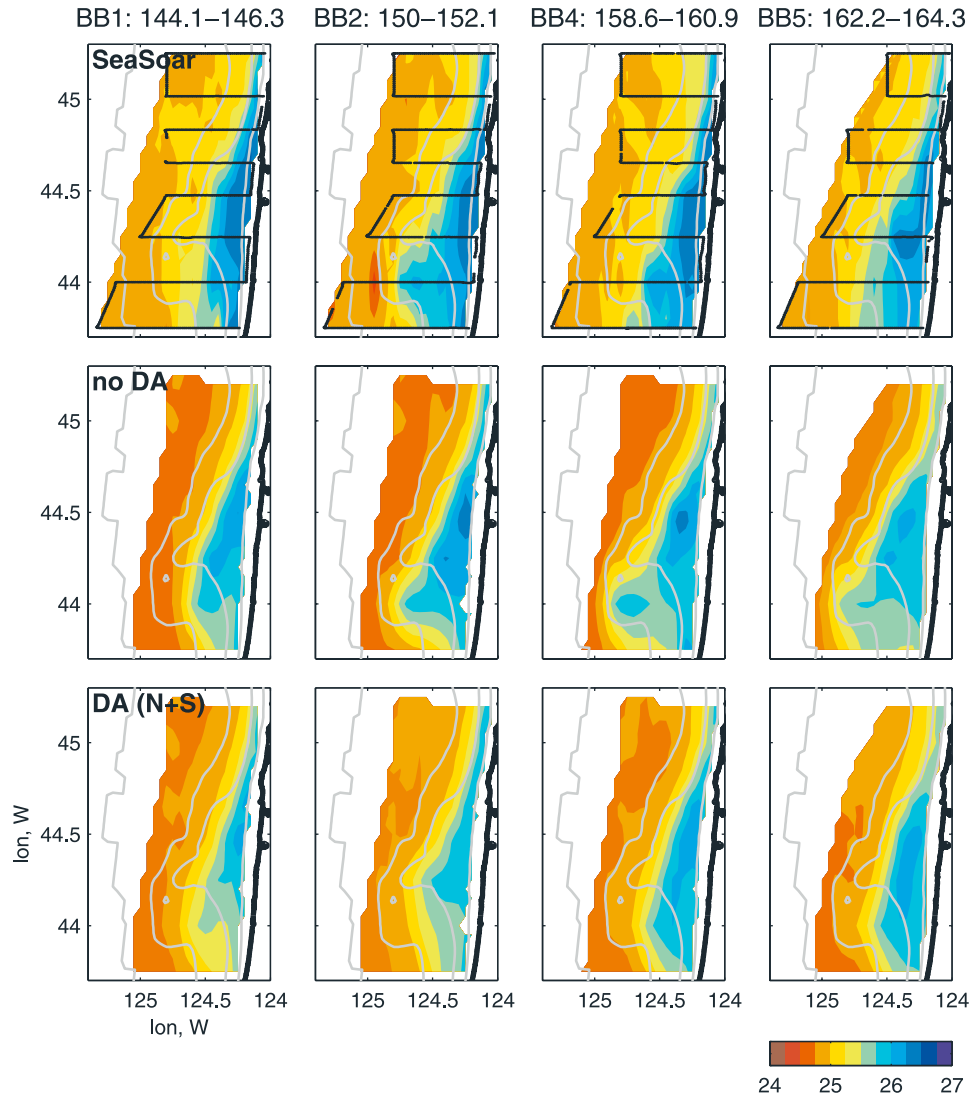

Figure 11. Potential density (kg m^{-3}) at 35 m, from (top) observed SeaSoar BB surveys, (middle) model only, and (bottom) DA (N+S). Survey times (yeardays) are shown above the SeaSoar plots. Bathymetric contours are at 50, 100, 200, and 1000 m. Cruise tracks are shown in upper plots. The model fields are constructed using the same sampling strategy as the SeaSoar surveys.

actual σ_θ values. In those cases, direct assimilation of temperature and salinity data may be necessary to place a stronger constraint on density structure.

[29] The model without DA reproduces qualitatively the upwelled isopycnal structure observed in the SeaSoar data. Velocity data assimilation affects the details of the density distribution and improves statistical comparisons of the model to data, but does not always lead to visible qualitative improvements. To the extent that success in this part of our study is limited, it raises critical issues with regard to the OI data assimilation approach used here. Results obtained from OI in this study should provide an important benchmark when more rigorous DA methods, which allow for a state-dependent $\mathbf{P}^f$, are applied to these data sets.

7. Sea Surface Salinity Transport

[30] Assimilation of moored velocities affects modeled transport of surface buoyant water. To illustrate this, some DA computations have been performed using both velocity and salinity data from sensors on the COAST moorings. Salinity measurements are available at NSB at depths of 11, 59, and 119 m below sea surface, NMS (1.5, 28, 70 m), NIS (12, 40 m), SSB (2.4, 9, 57, 117 m), SMS (10, 26, 88 m), and SIS (12, 40 m). Observational time series of S at the sensors closest to the surface for each mooring are shown in Figure 15 (shaded lines). Note that the sensors are actually very near the surface only at NMS (1.5 m) and SSB (2.4 m). Columbia River effects ($S < 32.5$ psu) are most pronounced during the first part of the study period, when they can be seen not only on line N (140 km south of the river mouth), but also at the southern sites SSB and SMS (230 km south of the river mouth).

[31] In case DA (N+S, Salt N) we assimilate, in addition to the velocity data from the 6 COAST moorings, salinity data from all eight sensors of line N. In a sense, in this part of our study salinity is used as a proxy for a buoyant tracer, and DA is used as a way to release this tracer on line N. The

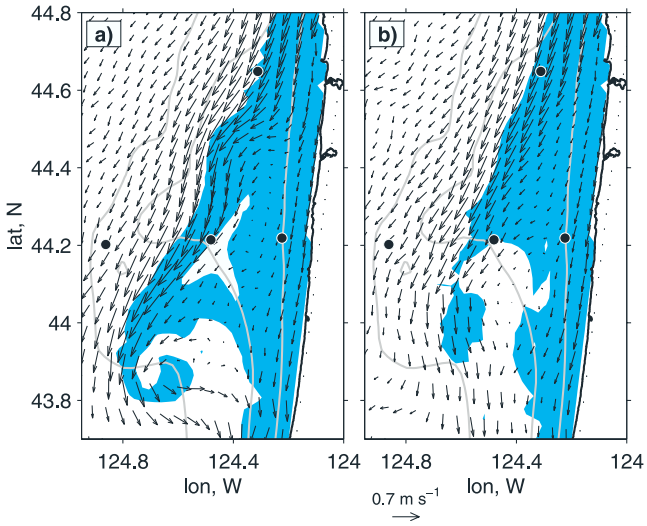

Figure 12. Snapshots of surface velocity (vectors) and surface σ_θ < 24.4 kg m^{-3} (shaded) on day 152.0 in the vicinity of Stonewall and Heceta Banks: (a) model without DA; (b) case DA (N+S). Bathymetric contours are 50, 100, and 200 m. Circles show mooring locations (NH10 and line S).

goal is to see if variability at the near-surface salinity sensor sites of line S is improved as a result of DA, especially at SSB and SMS that are on the path of the upwelling jet. In Figure 15, time series for S from the DA model are shown as solid black lines. The model-data salinity RMS errors and correlations at the near-surface sensor locations on line S are given in Table 3.

[32] Assimilation of S requires specification of the forecast error covariance $\mathbf{P}^f$ corresponding to these data. Computation of $\mathbf{P}^f$ involved, as an initial step, the estimation of a covariance of errors in the model using the statistical analysis of the same ensemble of model runs as that of K05. Salinity variability in that ensemble is caused by upwelling processes, rather than Columbia River outflow. Such a covariance may have reasonable horizontal spatial structure (e.g., higher expected covariability in the direction of the upwelling jet), but may be less realistic in the vertical. Indeed we find that although salinity DA can improve prediction of near-surface S, it may corrupt the density structure at depth, e.g., in terms of statistical parameters discussed in the previous section.

[33] The model without DA (dotted line in Figure 15) shows significantly lower variability and higher salinity values than observations, since river outflow is not included in the model. So it is not a big surprise that case DA (N+S, Salt N) provides a significantly better solution for near-surface S at SSB and SMS than a no DA case. To further illustrate the value of moored velocity assimilation on surface salinity transport, case DA (N+S, Salt N) is also compared against case DA (Salt N), where only salinity data at line N, but no velocities are assimilated (dashed line in Figure 15). In this case, improvement in salinity at SSB is comparable to that in case DA (N+S, Salt N) (see Table 3). However, the result is different at SMS at 10 m, where combined velocity and salinity assimilation [Case DA (N+S, Salt N)] significantly improves salinity variability at SMS at 10 m, but case DA (Salt N) does not.

[34] At SIS, located in the jet separation zone, the model-data salinity correlation is improved similarly at 12 m below the surface as a result of DA in both cases, DA (N+S, Salt N) and DA (Salt N). However, the salinity model-data RMS error at SIS is worse in both DA cases than in the model without DA. Apparently, the DA unrealistically freshens nearshore water at line S. As discussed by K05, the forecast error covariance for inshore sites may have an artificially long spatial scale. Model runs used for covariance estimation were forced with spatially uniform winds, resulting in alongshore uniform behavior close to the coast, where dynamics is strongly affected by the local wind. By virtue of this long spatial scale, waters near SIS are freshened when correction for the river effect is made using data on line N. This situation again demonstrates that the model should be refined to include more realistic forcing (spatially variable wind and river outflow), in order to improve $\mathbf{P}^f$.

[35] Overall, these experiments show that assimilation of velocities improves the transport of surface buoyant water associated with the Columbia River. Solution DA (N+S, Salt N) provides an adequate description of surface salinity variability between the mooring lines in the first half of the study period when a series of Columbia River water intrusion events occur. This conclusion is corroborated by a comparison with Big Box salinity maps at 5 m depth. Standard deviations of model-data differences StD($S^m - S^o$) and model-data correlations Corr(S^m, S^o) are given in Figure 16. In this analysis, we use SeaSoar salinity data between latitudes 43.7°–45.2°N (SeaSoar cross-shore lines 2–8) and for shelf depths >50 m. During

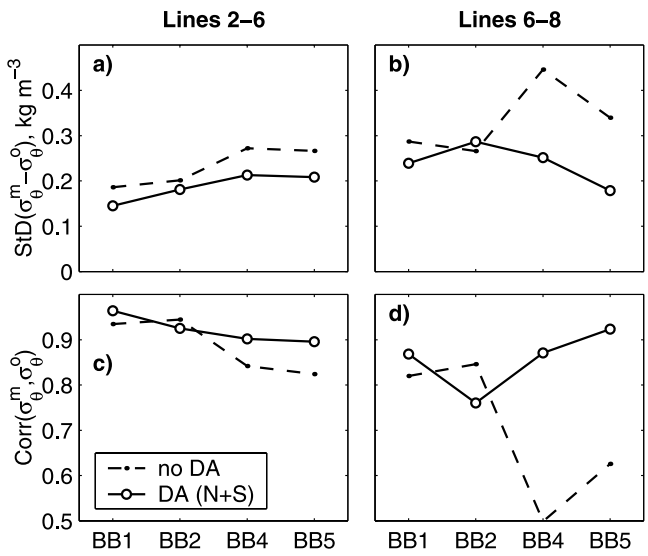

Figure 13. Model-data statistics for σ_θ using SeaSoar CTD data from four BB surveys at 35 m below the sea surface (see Figure 11) over shelf depths 50–200 m, model without DA (dashed lines), and velocity DA (N+S) (solid lines). (top) Standard deviations of model-observation differences. (bottom) Model-data correlations. (left) BB lines 2–6 (44.2°–45.0°N). (right) BB lines 6–8 (43.7°–44.2°N).

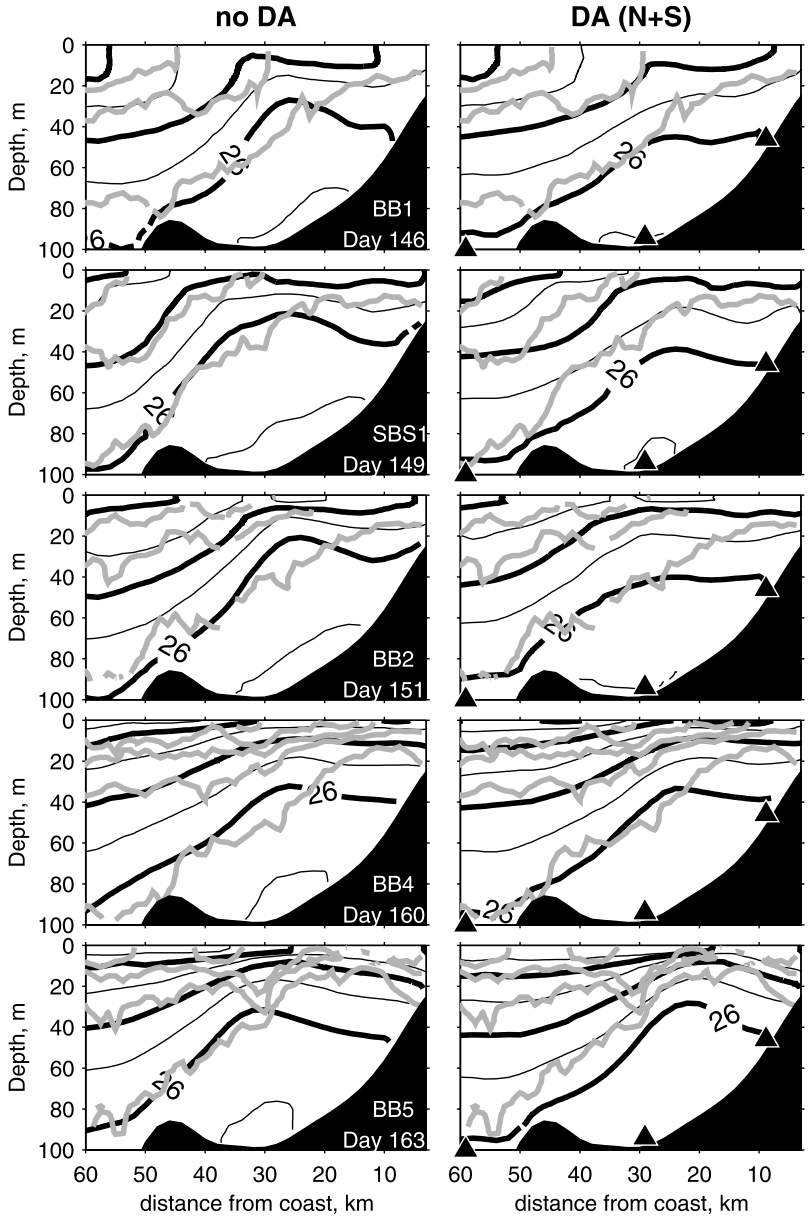

Figure 14. Contours of potential density σ_θ near line S (44.2°N) on five different days: (left) model without data assimilation and (right) DA (N+S). Modeled contours are in black, with contour interval 0.5 kg m^{-3}. Shaded contours are from SeaSoar observed hydrographic sections, with contour intervals 1 kg m^{-3} (the deepest contoured SeaSoar isopycnal is at 26 kg m^{-3}). Triangles mark mooring locations.

survey BB1 (days 144.1–146.3), when the presence of Columbia water is not evident in the mooring salinity data (see Figure 15), statistics for the model only and DA cases are close. Model-data correlations are high (>0.9) (Figure 16), since spatial variability both in the data and the model is dominated by the large contrast in S between inshore and shelf break areas. Surveys BB2, BB4, and BB5 are performed during significant fresh water intrusion. During these times, correlation of observed and modeled (no DA) salinity values drops significantly. Joint velocity and salinity DA [case DA(N+S, Salt N)] improves StD($S^m - S^o$) and Corr(S^m, S^o), compared with the no DA case or case DA (Salt N).

[36] An example of observational and modeled salinity maps at 5 m below sea surface is given in Figure 17 for survey BB5 (days 162.2 to 164.3). The map from solution DA (N+S, Salt N), again sampled similar to the observations, is qualitatively similar to the SeaSoar map, with a distinctive pattern of areas of fresher and saltier water (Figures 17a and 17b). In the south (e.g., at 44°N), the freshened water is found offshore, separated from the coast by an area of saltier water. In the north (at 45°N), Columbia river water is observed and modeled to be near shore. Neither the model without DA, which does not have Columbia river discharge (Figure 17c), nor the case DA (Salt N) (Figure 17d) reproduces this pattern of spatial variability.

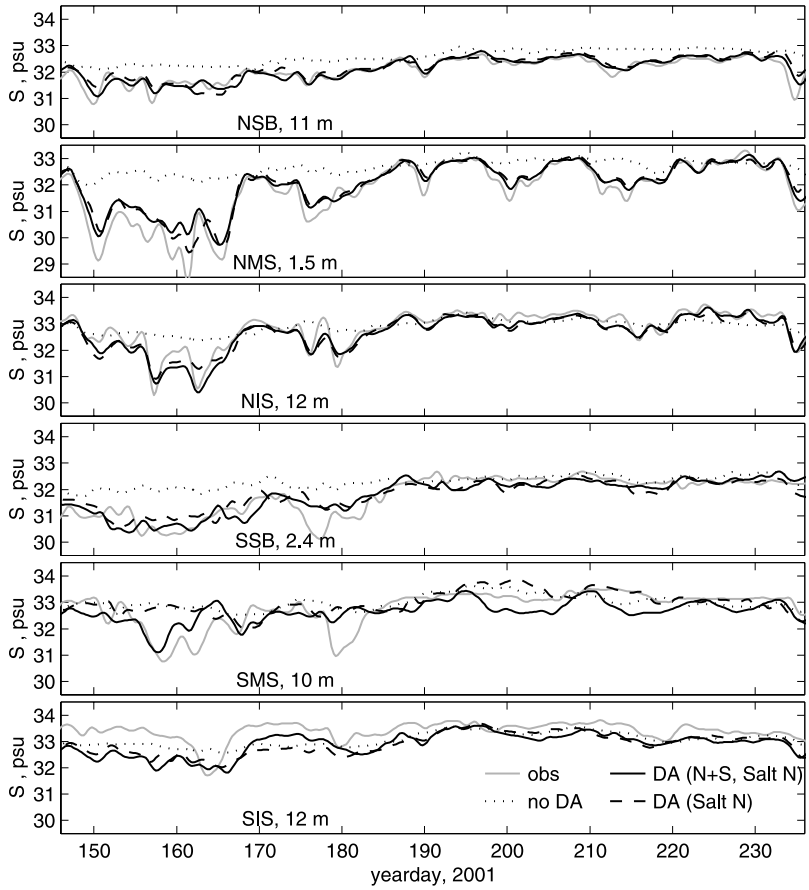

Figure 15. Time series of salinity at the moorings on lines N and S at the depths of the sensors closest to the sea surface: observed (shaded lines), model only (dotted lines), DA (N+S, Salt N) (solid lines), and DA (Salt N) (dashed lines). The model-data statistics for the southern sites are given in Table 3.

[37] Note it took over 2 days to complete survey BB5. It started in the southeast during the peak of northward, downwelling favorable wind. As the survey progressed the wind changed to southward, upwelling favorable (see Figure 2). So, the southern parts of maps in Figures 17a and 17b are likely to be representative of summer downwelling, while the northern parts show the beginning of an upwelling event. In the beginning of this survey, during downwelling, the alongshore current was toward the north on the inner shelf, but continued flowing southward farther offshore. This caused significant dispersion of the sea surface water associated with Columbia River intrusion. From a Lagrangian analysis using surface current fields, we determine that in these downwelling conditions surface passive tracer particles released at midshelf (e.g., near site SMS) on day 162 will separate at the rate of 25 km d^{-1} in the direction along the coast and at the same time be transported onshore. Maximum separation rates have similar magnitudes in cases with and without DA, but DA changes the spatial distribution of the zones of larger separation.

8. Data Assimilation Effect on Near-Bottom Turbulence Parameters

[38] Data assimilation can affect variability in bottom boundary layer (BBL) processes by correcting near-bottom velocities. In this section, comparisons between the model and observations are made for the level and temporal variability of the turbulent dissipation rate ε in the BBL and of the bottom stress magnitude τ_B.

[39] During days 139–148 of 2001, high-resolution profiling of small-scale velocity gradients, temperatures, and conductivity was performed from the R/V *Thompson* in a cross-shore section at 45°N [*Moum et al.*, 2005]. This

Table 3. Salinity Model-Data RMS Error (psu) and Correlation for Days 146–191 at Mooring Sensor Locations Closest to the Surface, Line S

	SSB, 2.4 m		SMS, 10 m		SIS, 12 m	
Case	RMS Error	Correlation	RMS Error	Correlation	RMS Error	Correlation
No DA	1.07	0.56	0.83	0.30	0.56	0.57
DA (N+S, Salt N)	0.43	0.75	0.58	0.57	0.73	0.66
DA (Salt N)	0.48	0.72	0.81	0.10	0.76	0.70

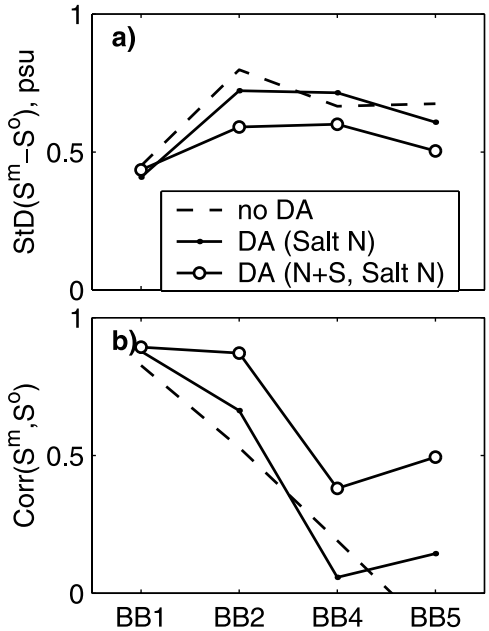

Figure 16. Statistics for salinity S at 5 m below the sea surface comparing the model and SeaSoar CTD data from four BB surveys. The data are selected at shelf depths >50 m, latitudes 43.7°–45.2°N (which include BB lines 2–8, see Figure 17). Model cases are no DA (dashed lines), case DA (Salt N) (solid lines with dot symbols), and DA (N+S, Salt N) (solid lines with open circles): (a) standard deviation of model-observation differences and (b) model-data correlation.

location was chosen because of its simple topography, so that observed effects might be interpreted using theoretical analysis in two spatial dimensions (depth and cross-shore coordinates). The transect was repeated twelve times at the same location across the continental shelf, capturing temporal variability in the BBL during two upwelling events bounding a period of relaxation from upwelling to downwelling. Turbulent dissipation rates for the observations were computed from the measured velocity gradients as by *Moum et al.* [1995].

[40] POM involves integration of prognostic equations for q^2 and q^2l, where q^2 is twice the turbulent kinetic energy and l is the turbulence length scale [*Mellor and Yamada*, 1982; *Galperin et al.*, 1988; *Mellor*, 2001]. The turbulent dissipation rate for the model is approximated as $\varepsilon = q^3/(16.6\, l)$, where units are m s^{-1} for q and meters for l.

[41] Sections of observed and modeled ε during transect 1 (centered on day 139.3) are shown in Figure 18. Observed (Figure 18a) and simulated (Figures 18b and 18c) levels of ε are comparable near the surface and bottom. Away from the surface and bottom boundaries the modeled ε is much lower than the observed background, in part because superinertial variability (e.g., tides and energetic inertial oscillations) are not forced in the model. In this transect, the model without DA (Figure 18b) has an apparently thinner BBL than the DA case (N+S) (Figure 18c).

[42] Availability of a 9 day series of turbulence measurements offers a rare opportunity to assess whether DA helps to improve temporal variability in the BBL ε. To compare the DA model to the full series of turbulence observations, a special DA case is run assimilating currents from NMS and NIS beginning on day 139. Observations at mooring NSB are not used since data acquisition there was started only on day 141. Because the comparison with the turbulence measurements is limited to the early days of the study period (days 139–148), a longer spin-up, 26 days before the start of assimilation, including 11 days with realistic winds, is used in this case.

[43] In Figure 19a, observed and modeled BBL ε are compared, averaged over the bottom 25 m and in a horizontal range of bathymetric depths from 50 to 170 m (i.e., the box in Figure 18). The observational line (dotted line with boxes) has three maxima in the near-bottom ε (the first and the third corresponding to upwelling events and the second to relaxation from upwelling to downwelling). In Figure 19a, the third maximum is not as apparent as the preceding two, since during the relatively short second upwelling event the higher near-bottom ε was confined to depths <100 m. This maximum is more apparent if horizontal averaging is restricted to bathymetric

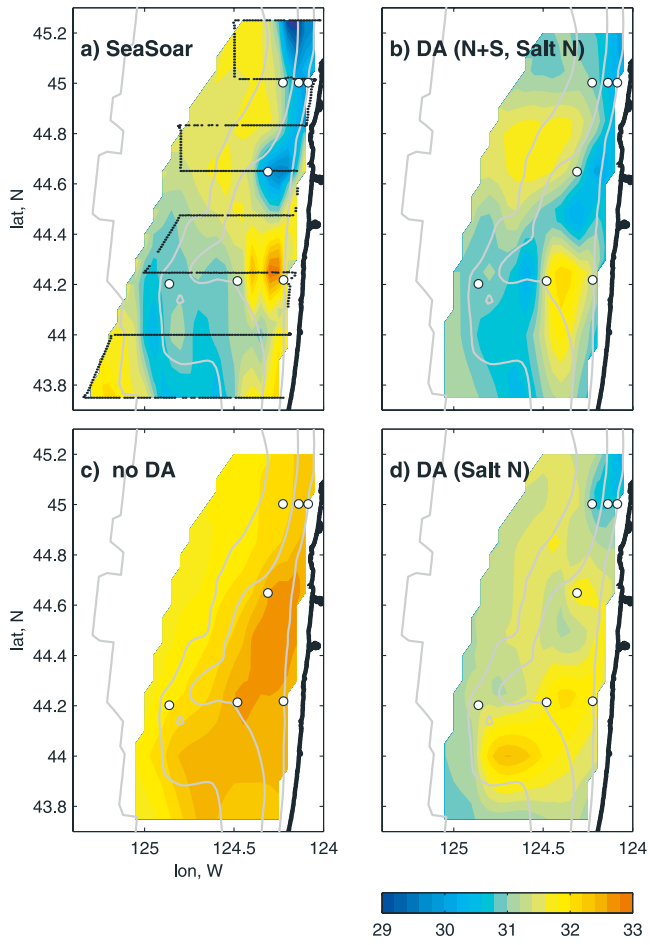

Figure 17. Salinity (psu) at 5 m depth during SeaSoar survey BB5, days 162.2–164.3: (a) SeaSoar data, with the cruise track (dotted line) originating in the southeast; (b) solution DA (N+S, Salt N); (c) no DA solution; (d) DA (Salt N). Model maps are plotted using the same sampling strategy as the SeaSoar survey. Bathymetry contours are at 50, 100, 200, and 1000 m. Circles show mooring locations.

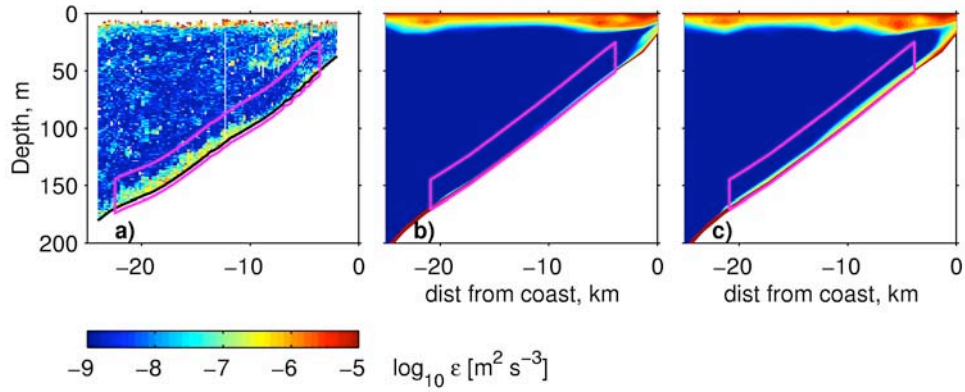

Figure 18. Turbulent dissipation rate in a cross-shore section on line N, section time centered on day 139.3: (a) observations, transect 1 [*Moum et al.*, 2005]; (b) model without DA; (c) DA (N+S). The box near the bottom shows an area of averaging for model-data comparison (Figure 19a).

depths 50–100 m (Figure 19b). In both Figures 19a and 19b, the model without DA (thin line) does not reproduce the observed pattern of variability, predicting the first maximum late, missing the second, and dissipating too much energy on the third event. The DA constrains the magnitude and direction of velocities in the BBL and reproduces all three events with comparable mean levels of ε at their peaks. During periods of local minima in ε, model dissipation values in the BBL are closer to the background level above it, such that area-averaged modeled values are lower than observed. In terms of statistical parameters, the model-data correlation for the records in Figure 19a improved from −0.34 (no DA) to 0.67 (DA), and the RMS error improved from 2.7×10^{-7} (no DA) to 0.58×10^{-7} m^2 s^{-3} (DA).

[44] Model skill in predicting the bottom stress magnitude τ_B is also assessed, since it is an important variable for the behavior of shelf circulation models. In the cross section at latitude 45°N, model estimates [cases with no DA and DA (NMS+NIS)] are compared to values calculated from measured ε using the dissipation method [*Perlin et al.*, 2005] (Figure 20). Qualitatively, data assimilation brings the modeled and observational τ_B in closer agreement on most transects. Similar to results for ε, velocity data assimilation improves the level and temporal variability in τ_B averaged in the cross-shore direction (see Figure 21a). The model-data RMS error and the standard deviation of model-data differences (Figures 21b and 21c) are improved for most transects. Note that the standard deviation is a measure of how close trends in the lines of Figure 20 are.

[45] In terms of the above mentioned criteria, data assimilation does not provide improvement to τ_B in transects 7 and 8 (days 143.5–144.5), during relaxation from upwelling to downwelling conditions. Possible reasons for poorer model performance during downwelling include insufficient horizontal resolution. For instance, a modeling study in a two-dimensional setup (variations in the vertical and cross-shore) using the bathymetry of the 45°N section and 250 m horizontal resolution [*Wijesekera et al.*, 2003] shows formation of a downwelling front, in which turbulence variables (e.g., ε) change significantly over a horizontal scale as small as 2 km. In that two-dimensional study the front was

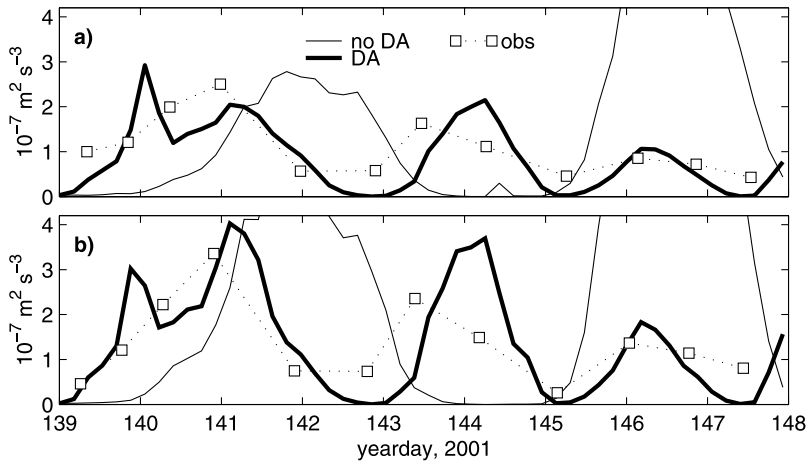

Figure 19. Comparisons of modeled and observed time series of near-bottom turbulent dissipation rate ε at 45°N averaged over the bottom 25 m and in a horizontal range of bathymetric depths from (a) 50 to 170 m or (b) 50 to 100 m. Thin lines are for the solution with no DA, bold lines are for case DA (NMS+NIS), and dotted lines with squares are for observations.

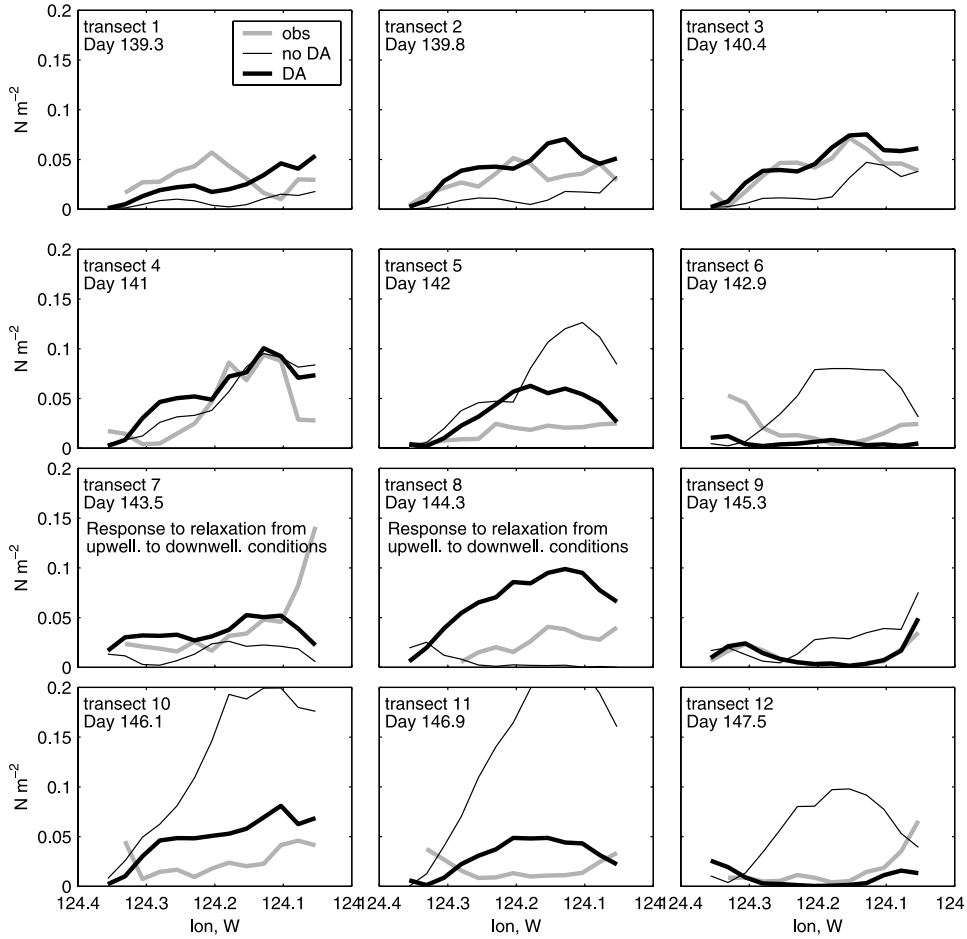

Figure 20. Bottom stress magnitude at 45°N from turbulence microstructure observations (shaded lines), model without DA (thin lines), and case DA (NMS+NIS) (bold lines). Model-data statistics are given in Figure 21.

formed at a distance of 8 km from the coast. Evidence of a front can be seen from the observed τ_B as a rise near the coast in Figure 20, transect 7. This sharp feature is not reproduced in our model. It is also true that the method of calculating τ_B from observed ε, assuming a balance between turbulent dissipation and shear production in the BBL [*Perlin et al.*, 2005], is less reliable at this location in downwelling conditions, when bottom mixing has been shown to be in part convectively driven [see *Moum et al.*, 2005]. Correlation of model and observational values of τ_B computed using values from all transects (Figure 20), except 7 and 8, is virtually 0 in the case of the model without DA and is 0.56 in the DA case.

[46] In the model without DA, the average level of τ_B for the period of model-data comparison is nearly twice as large as the observed level. Data assimilation reduces the model average to 20% above the observed level (with values for transects 7 and 8, corresponding to downwelling, excluded). The compared time series are too short to say with confidence that bottom stress values during upwelling are overestimated on average over the entire study period. It was shown by K05 that the depth- and time-averaged dynamical term balances in the direction along the jet include a DA correction term that in general retards the mean southward flow. The physical source for this term is yet to be determined. If the DA model indeed overestimates the bottom stress during upwelling, the DA correction term, which is on average the same sign as the bottom stress, cannot be associated solely with the bottom stress. As a possibility, the DA correction term could be associated with the form drag over small-scale bathymetry [*Nash and Moum*, 2001], unresolved in our model, or with the transfer of energy from the jet to frontal instabilities, as discussed by K05.

[47] In Figures 22a and 22b, the analysis of the near-bottom ε and τ_B at 45°N is continued for the entire study period (days 140–237) using the standard DA and no DA cases. For reference, the cross-shore (u) component of the bottom velocity near NMS is plotted in Figure 22c. Soon after the time of the last turbulence microstructure survey transect, the DA model shows two more significant events of high ε [downwelling on day 149 ($u < 0$) and upwelling on day 152 ($u > 0$)]. After that, the next events of comparable magnitude do not happen until day 167 (upwelling), and then day 179 (downwelling). Both of these events appear to be misrepresented in the model without DA (shaded line in Figure 22a). Also, DA restricts the dissipation rates during days 185–198, by constraining the magnitude of the southward current (see Figure 6). Both the DA and no DA cases show increased ε during days 214–220 following a pro-

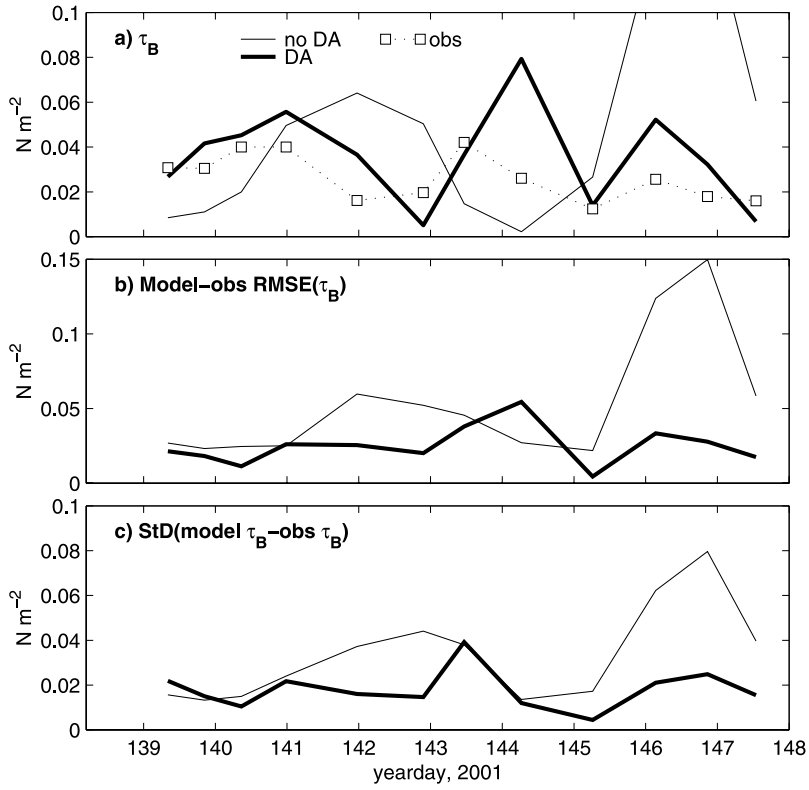

Figure 21. Comparisons of modeled and observed time series of the bottom stress magnitude τ_B by averaging in the cross-shore direction at 45°N: (a) average bottom stress τ_B, no DA (thin line), DA (NMS+NIS) (bold line), and observations (dotted line with squares); (b) model-data τ_B RMS error, no DA (thin line) and DA (NMS+NIS) (bold line); and (c) standard deviation of model-data τ_B differences.

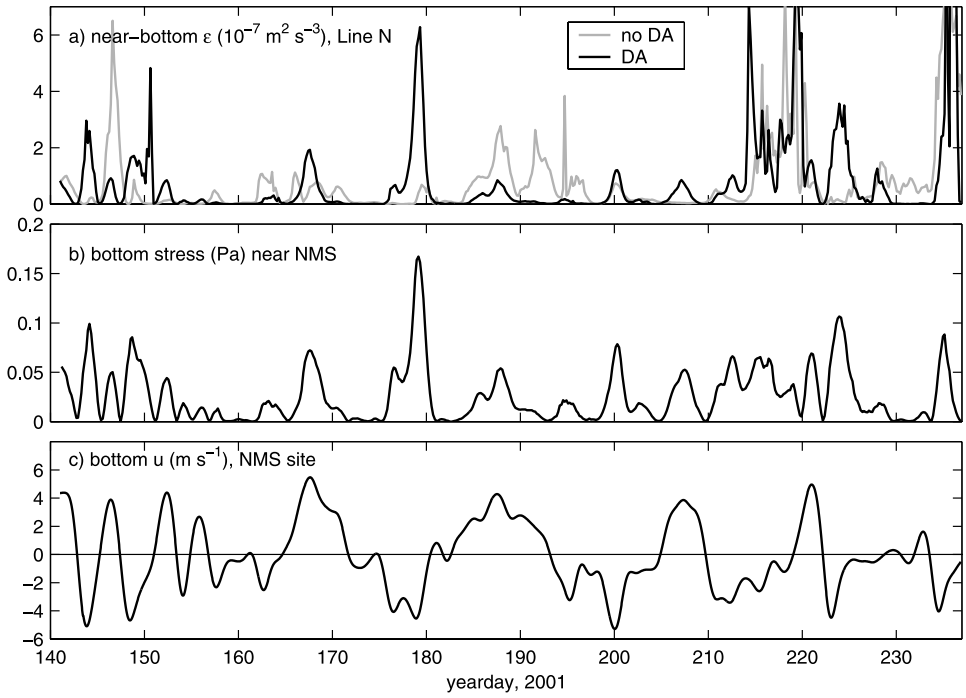

Figure 22. Time series of some near-bottom model variables in a section of line N plotted for the whole study period, case DA (N+S): (a) ε averaged vertically and across-shore in the area shown in Figure 18, with a shaded line corresponding to a model-only solution; (b) τ_B near NMS; (c) bottom u near NMS.

longed period of relaxation from upwelling to downwelling. Periods of increased τ_B coincide with those of increased ε. A more detailed analysis of the temporal and spatial variability in τ_B on the Oregon shelf is presented by *Kurapov et al.* [2005b].

9. Summary

[48] Extensive model-data comparisons have shown that assimilation of moored profiler velocities into a primitive equation model of wind-forced circulation on the Oregon shelf can improve the representation of the sea surface height, temperature, potential density gradients, surface salinity transport, the turbulent dissipation rate in the BBL and the bottom stress. Sequential assimilation of moored velocity measurements not only improves model-data statistics, but also implies dynamically significant changes of the circulation on the temporal scale of several days.

[49] The data assimilative model is thus shown to be a valuable tool for data synthesis, allowing observations, sparse in space and time, to be brought together to constrain the three-dimensional and time-dependent multivariate ocean state. Data that are not assimilated, but used for verification, raise our confidence in the model performance and provide an estimate of the solution error.

[50] Model-data comparisons involving high-resolution cross sections of potential density show that in an area of simple bathymetric slope with relatively weak alongshore variations the model (even without DA) provides a very good description of isopycnal structure, given appropriate initial conditions for T and S. In areas of more complicated bathymetry, velocity DA improves the model density gradients (isopycnal slopes), but not necessarily the actual density values. In those cases, direct assimilation of T and S data, e.g., from moorings or autonomous underwater vehicles (AUV), in addition to velocities, may place stronger constraints on density structure.

[51] Comparisons with turbulence microstructure data show that the subgrid turbulence parameterization in POM provides a reasonable description of the turbulent dissipation rate and bottom stress when DA is used to correct the resolved part of the current. These comparisons have shown a positive local effect of assimilation of velocities from moorings at 45°N. We lack a similar series of transects farther to the south to verify BBL ε and τ_B in the area between the two mooring lines. However, based on our understanding that improvement in these quantities is associated with correction of velocities near the bottom, we may expect that BBL variability is improved in the entire region between the mooring lines in case DA (N+S), since velocities are constrained by DA on lines N and S and significant improvement in (u, v) is verified to be obtained at NH10 throughout the water column. Supported by the model-data comparison described in this manuscript, the DA model can be utilized with increased confidence for future analysis of spatial and temporal variability in BBL processes on the mid-Oregon shelf [see *Kurapov et al.*, 2005b].

[52] An optimal interpolation (OI) DA method of the sort used here is relatively easy to implement with a complicated, fully nonlinear model like POM. It is useful for initial assessment of the value of the data in a DA system. However, OI is limited in that the forecast error covariance $\mathbf{P}^f$ does not change with time. The study of the effect of DA on the density structure in horizontal maps suggests that, while adequate on average, $\mathbf{P}^f$ may inhibit intermittent flow features like jet meandering and eddies with horizontal scales smaller than the decorrelation length scale implied by the time-averaged $\mathbf{P}^f$. In an example involving salinity data, we suggest that the spatial pattern of $\mathbf{P}^f$ corresponding to the S field should depend on whether error in the forecast of S is associated primarily with inadequate representation of river outflow or with error in the upwelling intensity. More complicated DA methods, for instance, those based on the use of an adjoint [*Chua and Bennett*, 2001], are free from the assumption that model error statistics are time-independent. Thus these more advanced DA methods may utilize observational information in a more complete way to enhance multivariate capabilities of a DA model. Work is presently in progress on the formulation and implementation of these advanced DA methods for the studies of coastal ocean circulation.

[53] **Acknowledgments.** This research was supported by the Office of Naval Research (ONR) Ocean Modeling and Prediction Program under grant N00014-98-1-0043, by the National Science Foundation (NSF) Coastal Ocean Processes (CoOP) program under grant OCE-9907854, and by the NSF GLOBEC Program under grant OCE-0000733. Authors wish to thank J. N. Moum for stimulating discussions concerning interpretation of the model-data turbulence comparisons and Robert O'Malley and Alexander Perlin for analysis of, and consultations on, SeaSoar and turbulence microstructure data. We also thank all the research assistants, marine technicians, and crews of the R/Vs Wecoma and Thomas G. Thompson for their efforts in obtaining the extensive data sets used in this analysis.

References

Barth, J. A., R. O'Malley, and A. Y. Erofeev (2003), SeaSoar observations during the Coastal Ocean Advances in Shelf Transport (COAST), Survey I: 23 May–13 June 2001, W0105C, *Data Rep. 191*, Coll. of Oceanic and Atmos. Sci. Oregon State Univ., Corvallis.

Beşiktepe, Ş. T., P. F. L. Lermusiaux, and A. Robinson (2003), Coupled physical and biochemical data driven simulations of Massachusetts Bay in late summer: Real-time and post-cruise data assimilation, *J. Mar. Syst.*, *40*, 171–212.

Blumberg, A. F., and G. L. Mellor (1987), A description of a three-dimensional coastal ocean circulation model, in *Three-Dimensional Coastal Ocean Models*, *Coastal Estuarine Sci. Ser.*, vol. 4, edited by N. Heaps, pp. 1–16, AGU, Washington, D. C.

Boyd, T., M. D. Levine, P. M. Kosro, S. R. Gard, and W. Waldorf (2002), Observations from moorings on the Oregon Continental Shelf, May–August 2001, *Ref. 2002-6, Data Rep. 190*, Oregon State Univ., Corvallis.

Breivik, Ø., and Ø. Sætra (2001), Real time assimilation of HF radar currents into a coastal ocean model, *J. Mar. Syst.*, *28*, 161–182.

Castelao, R. M., and J. A. Barth (2005), Coastal ocean response to summer upwelling favorable winds in a region of alongshore bottom topography variations off Oregon, *J. Geophys. Res.*, *110*, C10S04, doi:10.1029/2004JC002409.

Chen, C.-S., and D.-P. Wang (1999), Data assimilation study of the Santa Barbara Channel circulation, *J. Geophys. Res.*, *104*, 15,727–15,741.

Chua, B. S., and A. F. Bennett (2001), An ocean inverse system, *Ocean Modell.*, *3*, 137–165.

Daley, R. (1993), *Atmospheric Data Analysis*, 455 pp., Cambridge Univ. Press, New York.

Freeland, H. J., G. Gatien, A. Huyer, and R. L. Smith (2003), Cold halocline in the northern California Current: An invasion of subarctic water, *Geophys. Res. Lett.*, *30*(3), 1141, doi:10.1029/2002GL016663.

Galperin, B., L. H. Kantha, S. Hassid, and A. Rosati (1988), A quasi-equilibrium turbulent energy model for geophysical flows, *J. Atmos. Sci.*, *45*, 55–62.

Gan, J., and J. S. Allen (2002), A modeling study of shelf circulation off northern California in the region of the Coastal Ocean Dynamics Experiment: Response to relaxation of upwelling winds, *J. Geophys. Res.*, *107*(C9), 3123, doi:10.1029/2000JC000768.

Gan, J., and J. S. Allen (2005), On open boundary conditions for a limited-area coastal model off Oregon. part 1: Response to idealized wind forcing, *Ocean Modell.*, *8*, 115–133, doi:10.1016/j.ocemod2003.12.006.

Gan, J., J. S. Allen, and R. M. Samelson (2005), On open boundary conditions for a limited-area coastal model off Oregon. part 2: Response to wind forcing from a regional mesoscale atmospheric model, *Ocean Modell.*, *8*, 155–173, doi:10.1016/j.ocemod2003.12.007.

Kundu, P. K. (1976), Ekman veering observed near the ocean bottom, *J. Phys. Oceanogr.*, *6*, 238–242.

Kurapov, A. L., G. D. Egbert, R. N. Miller, and J. S. Allen (2002), Data assimilation in a baroclinic coastal ocean model: Ensemble statistics and comparison of methods, *Mon. Weather Rev.*, *130*, 1009–1025.

Kurapov, A. L., G. D. Egbert, J. S. Allen, and R. N. Miller (2003), M_2 internal tide off Oregon: Inferences from data assimilation, *J. Phys. Oceanogr.*, *33*, 1733–1757.

Kurapov, A. L., J. S. Allen, G. D. Egbert, R. N. Miller, P. M. Kosro, M. Levine, and T. Boyd (2005a), Distant effect of assimilation of moored currents into a model of coastal wind-driven circulation off Oregon, *J. Geophys. Res.*, *110*, C02022, doi:10.1029/2003JC002195.

Kurapov, A. L., J. S. Allen, G. D. Egbert, and R. N. Miller (2005b), Modeling bottom mixed layer variability on the mid-Oregon shelf during summer upwelling, *J. Phys. Oceanogr.*, *35*, 1629–1649.

Lewis, J. K., I. Shulman, and A. F. Blumberg (1998), Assimilation of Doppler radar current data into numerical ocean models, *Cont. Shelf Res.*, *18*, 541–559.

Mellor, G. L. (2001), One-dimensional, ocean surface layer modeling: A problem and a solution, *J. Phys. Oceanogr.*, *31*, 790–809.

Mellor, G. L., and T. Yamada (1982), Development of a turbulent closure model for geophysical fluid problems, *Rev. Geophys.*, *20*, 851–875.

Moum, J. N., M. C. Gregg, R. C. Lien, and M. E. Carr (1995), Comparison of turbulence kinetic energy dissipation rate estimates from two ocean microstructure profilers, *J. Atmos. Oceanic Technol.*, *12*, 346–366.

Moum, J. N., A. Perlin, J. M. Klymak, M. D. Levine, T. Boyd, and P. M. Kosro (2005), Convectively-driven mixing in the bottom boundary layer, *J. Phys. Oceanogr.*, *34*, 2189–2202.

Nash, J. D., and J. N. Moum (2001), Internal hydraulic flows on the continental shelf: High drag states over a small bank, *J. Geophys. Res.*, *106*, 4593–4612.

Oke, P. R., J. S. Allen, R. N. Miller, G. D. Egbert, and P. M. Kosro (2002a), Assimilation of surface velocity data into a primitive equation coastal ocean model, *J. Geophys. Res.*, *107*(C9), 3122, doi:10.1029/2000JC000511.

Oke, P. R., J. S. Allen, R. N. Miller, G. D. Egbert, J. A. Austin, J. A. Barth, T. J. Boyd, P. M. Kosro, and M. D. Levine (2002b), A modeling study of the three-dimensional continental shelf circulation off Oregon, I, Model-data comparisons, *J. Phys. Oceanogr.*, *32*, 1360–1382.

Oke, P. R., J. S. Allen, R. N. Miller, and G. D. Egbert (2002c), A modeling study of the three-dimensional continental shelf circulation off Oregon, II, Dynamical balances, *J. Phys. Oceanogr.*, *32*, 1383–1403.

Perlin, A., J. N. Moum, J. M. Klymak, M. D. Levine, T. Boyd, and P. M. Kosro (2005), A modified law-of-the-wall applied to oceanic bottom boundary layers, *J. Geophys. Res.*, *110*, C10S10, doi:10.1029/2004JC002310.

Stammer, D., C. Wunsch, R. Giering, C. Eckert, P. Heimbach, J. Marotzke, A. Adcroft, C. N. Hill, and J. Marshall (2003), Volume, heat, and freshwater transports of the global ocean circulation 1993–2000, estimated from a general circulation model constrained by World Ocean Circulation Experiment (WOCE) data, *J. Geophys. Res.*, *108*(C1), 3007, doi:10.1029/2001JC001115.

Wheeler, P. A., A. Huyer, and J. Fleischbein (2003), Cold halocline, increased nutrients and higher chlorophyll off Oregon in 2002, *Geophys. Res. Lett.*, *30*(15), 8021, doi:10.1029/2003GL017395.

Wijesekera, H. W., J. S. Allen, and P. A. Newberger (2003), Modeling study of turbulent mixing over the continental shelf: Comparison of turbulent closure schemes, *J. Geophys. Res.*, *108*(C3), 3103, doi:10.1029/2001JC001234.

Wong, K.-C., and A. Valle-Levinson (2002), On the relative importance of the remote and local wind effects on the subtidal exchange at the entrance to the Chesapeake Bay, *J. Mar. Res.*, *60*, 477–498.

J. S. Allen, J. A. Barth, T. Boyd, G. D. Egbert, P. M. Kosro, A. L. Kurapov, M. D. Levine, and R. N. Miller, College of Oceanic and Atmospheric Sciences, Oregon State University, 104 COAS Administrative Building, Corvallis, OR 97331, USA. (jallen@coas.oregonstate.edu; barth@coas.oregonstate.edu; tboyd@coas.oregonstate.edu; egbert@coas.oregonstate.edu; kosro@coas.oregonstate.edu; kurapov@coas.oregonstate.edu; levine@coas.oregonstate.edu; miller@coas.oregonstate.edu)